JGS
Journal of the Geological Society

Research article

Published online January 30, 2020 https://doi.org/10.1144/jgs2019-142 | Vol. 177 | 2020 | pp. 1057–1073

The nature and age of basement host rocks and fissure fills in the Lancaster field fractured reservoir, West of Shetland

R. E. Holdsworth[1,2]*, R. Trice[3], K. Hardman[1], K. J. W. McCaffrey[1,2], A. Morton[4,5], D. Frei[6], E. Dempsey[7], A. Bird[7] & S. Rogers[8]

[1] Department of Earth Sciences, Durham University, Durham DH1 3LE, UK
[2] Geospatial Research Ltd, Durham DH1 4EL, UK
[3] Hurricane Energy plc, Godalming GU7 2QN, UK
[4] HM Research, St Ishmaels SA62 3TJ, UK
[5] CASP, University of Cambridge, Cambridge CB3 0UD, UK
[6] Department of Earth Sciences, University of the Western Cape, 7530 Bellville, South Africa
[7] Department of Geography, Geology and Environment, University of Hull, Hull HU6 7RX, UK
[8] Golder Associates Ltd, Vancouver, BC, V5M 0C4 Canada

REH, 0000-0002-3467-835X; KJWM, 0000-0002-9882-1709; AM, 0000-0001-5649-4183; DF, 0000-0002-3734-737X; AB, 0000-0002-2496-4344; SR, 0000-0003-1234-0355

* Correspondence: r.e.holdsworth@durham.ac.uk

Abstract: Hosting up to 3.3 billion barrels of oil in place, the upfaulted Precambrian crystalline rocks of the Lancaster field, offshore west of Shetland, give key insights into how fractured hydrocarbon reservoirs can form in such old rocks. The Neoarchean (*c.* 2700–2740 Ma) charnockitic basement is cut by deeply penetrating oil-, mineral- and sediment-filled fissure systems seen in geophysical and production logs and thin sections of core. Mineral textures and fluid inclusion geothermometry suggest that a low-temperature (<200°C) near-surface hydrothermal system is associated with these fissures. The fills help to permanently prop open fissures in the basement, permitting the ingress of hydrocarbons into extensive well-connected oil-saturated fracture networks. U–Pb dating of calcite mineral fills constrains the onset of mineralization and contemporaneous oil charge to the mid-Cretaceous and later from Jurassic source rocks flanking the upfaulted ridge. Late Cretaceous subsidence and deposition of mudstones sealed the ridge, and was followed by buoyancy-driven migration of oil into the pre-existing propped fracture systems. These new observations provide an explanation for the preservation of intra-reservoir fractures ('joints') with effective apertures of 2 m or more, thereby highlighting a new mechanism for generating and preserving fracture permeability in sub-unconformity fractured basement reservoirs worldwide.

Supplementary material: Analytical methods and isotopic compositions and ages are available at https://doi.org/10.6084/m9.figshare.c.4763237

Thematic Collection: This article is part of the Geology of Fractured Reservoirs collection available at: https://www.lyellcollection.org/cc/the-geology-of-fractured-reservoirs

Received 2 September 2019; **revised** 1 November 2019; **accepted** 22 November 2019

More than 125 hydrocarbon fields with fractured basement reservoirs have been recognized worldwide (e.g. P'an 1982; Koning 2003; Cuong & Warren 2009; Gutmanis 2009; Trice 2014), but their geology and the processes that lead to the accumulation of significant volumes of hydrocarbons are poorly understood. In most basement plays, oil is thought to migrate from an organic-rich mudstone source rock into a trap formed from a palaeo-high, termed a 'buried hill' trap (Biddle & Wielchowsky 1994). The seal is typically provided by a blanketing sequence of clay-rich mudstone and the reservoir formed from naturally fractured crystalline basement rocks.

Given the very low matrix permeability of most basement rocks, oil and other associated fluids are typically transported and stored via well-connected, open fracture systems. The geological characteristics and formation mechanisms of these fracture systems are reservoir specific and are challenging to characterize as the fracture network (or hydrodynamic fracture network associated with fluid transportation) cannot be imaged directly using seismic reflection data. Borehole images and core samples can give insights into the fracture network, particularly when integrated with dynamic data such as pressure transient analysis, interference and production logging data.

Since 2009, the exploration and initial development of Lancaster, the UK's first wholly basement-hosted hydrocarbon field, has involved the drilling of several wells, with extensive image logs, drill stem testing and the collection of more than 80 sidewall cores, in addition to the interpretation of 3D seismic reflection data. This has facilitated a detailed investigation of the hydrocarbon-bearing and other fracture systems within the basement. In this paper we present a summary of the main findings that have arisen from a study of these materials, with particular focus on the sidewall cores. Thin-section observations and U–Pb zircon geochronology allow the nature, absolute age and affinities of the Lancaster basement to be established with a high degree of confidence. Microstructural analysis and calcite U–Pb dating shed new light on the fault rock and fracture filling history of the crystalline hosts and how this has allowed the ingress and accumulation of large volumes of hydrocarbons. The acquired geological information gives detailed insights into the geological processes that contribute to the reservoir potential of fractured basement. The findings are relevant to all basement reservoirs where pre-existing fracture networks have been exploited in sub-unconformity settings. More generally, these new geological observations have wider implications for fractured

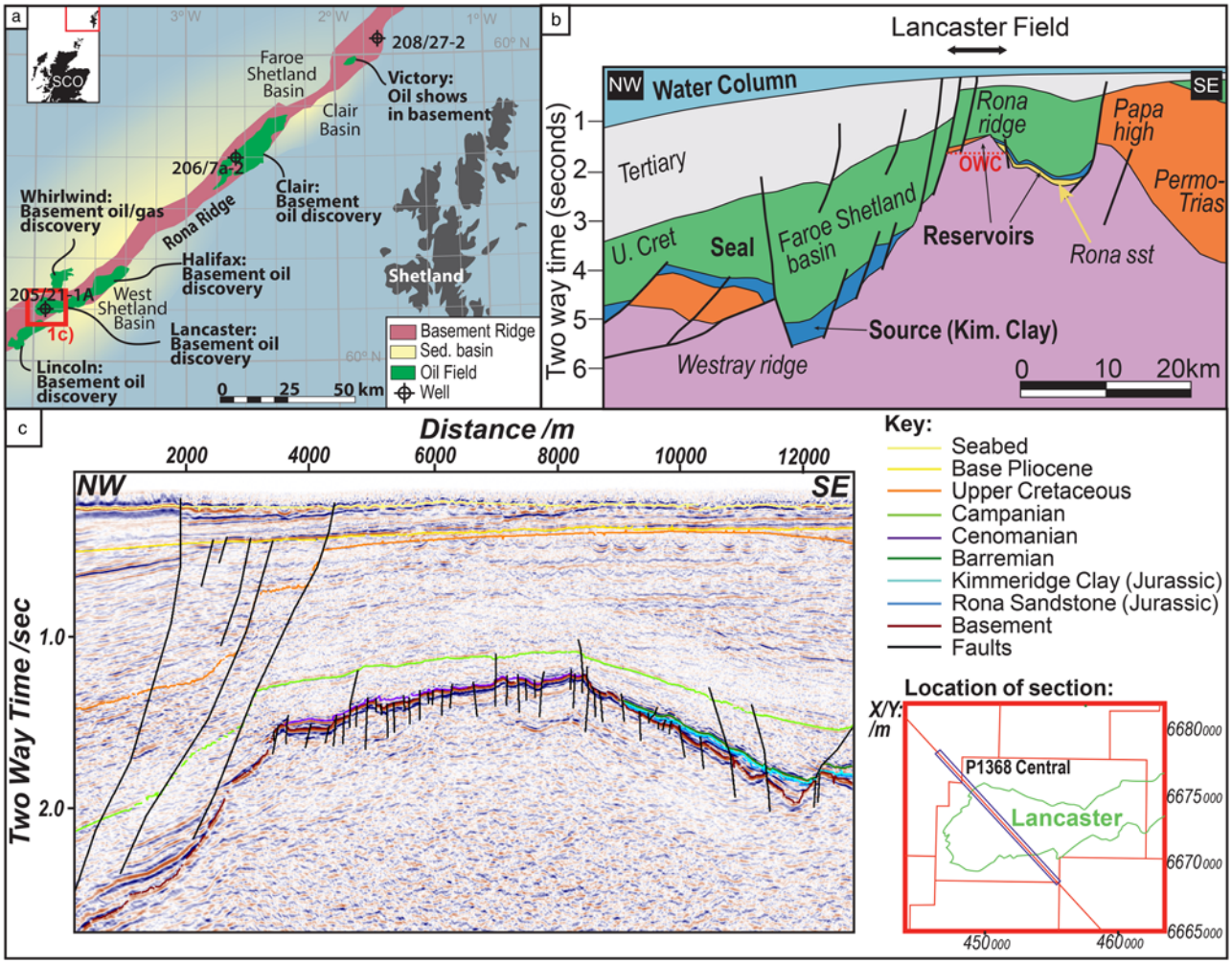

Fig. 1. (**a**) Simplified map showing location of Rona Ridge basement, oilfields and legacy wells referred to in this study. SCO, Scotland. The mapped extent of the Clair field includes the Devonian part of the reservoir (Clair Group). Red box shows location of map in (**c**). (**b**) Simplified NW0150SE cross-section through the Rona Ridge at Lancaster and the adjacent Faroe–Shetland Basin based on regional 2D seismic reflection profiles. (**c**) Interpreted NW–SE-trending seismic reflection profile across the Rona Ridge at Lancaster. Data courtesy of PGS (after Slightam 2012).

reservoirs and subsurface fluid migration processes worldwide, including in geothermal settings and basement aquifers.

Geological setting of the Lancaster field

The West of Shetland petroleum province (Fig. 1a) includes a number of significant but serendipitous oil discoveries made in wells drilled into basement along the Rona Ridge (e.g. 206/7a-2 (Clair); 205/21-1a (Lancaster); 208/27-2; Fig. 1a; Holdsworth *et al.* 2019). Some basement hosts, like those of the giant Clair field (6–7 billion barrels stock tank oil in place), underlie more conventional Devonian–Carboniferous sandstone reservoirs (Coney *et al.* 1993). Others, like those of the Lancaster and associated fields in the SW Rona Ridge, are hosted almost entirely within fractured basement (Fig. 1b and c; Slightam 2012; Trice 2014; Belaidi *et al.* 2016; total estimated oil in place >18 billion barrels).

Geochemical studies of oils from several fields along the Rona Ridge suggest a Late Jurassic Kimmeridge Clay source rock (Holmes *et al.* 1999; Finlay *et al.* 2011), thought to occur mainly on the downfaulted western flank of the ridge in the Faroe–Shetland Basin to the NW (Fig. 1b; Ritchie *et al.* 2011). Basin modelling and radioisotopic dating of oils and mineral fills in associated fractures suggest that oil maturation and associated hydrothermal mineralization in the Rona Ridge in the central and northeastern part of the Rona Ridge (Clair, Victory; Fig. 1a) occurred during a period of at least 25 myr in the Late Cretaceous (*c.* 90–65 Ma; Finlay *et al.* 2011; Holdsworth *et al.* 2019). It has been proposed that the oil progressively migrated from its Jurassic source via fracture systems propped open by partial Cretaceous-aged mineral and sediment fills up into the adjacent basement ridge and locally onward into cover sequences such as the Clair Group (Holdsworth *et al.* 2019). An alternative model might involve lateral and upward migration into an overlying Cretaceous carrier bed that drapes over the top of the Rona Ridge with downward filling into the fractured basement below (e.g. Psyrillos *et al.* 2003).

The *c.* 200 km long and 15 km wide Rona Ridge comprises a series of NE–SW-trending footwall blocks of Precambrian basement bounded by large Mesozoic normal faults with kilometre-scale offsets (Fig. 1a–c, Ritchie *et al.* 2011). Regional studies of basement cores west of Shetland reveal variably deformed assemblages of coarse-grained, upper amphibolite-facies granodioritic–dioritic plutons and orthogneisses that have yielded a narrow range of Neoarchean zircon ages (*c.* 2.83–2.73 Ga; Holdsworth *et al.* 2018). Broadly the same age as the protolith gneisses of the Lewisian Complex in Scotland, these rocks form part of the larger Faroe–Shetland Terrane located west of Shetland and can be correlated directly with rocks of the Rae Craton in Greenland and Canada (Kinny *et al.* 2019).

Regional 2D seismic reflection surveys and boreholes show that the basement ridge is immediately overlain by a diverse but volumetrically limited range of Late Paleozoic–Mesozoic cover sequences, with many lateral thickness variations and local unconformities (Fig. 1b and c; Ritchie *et al.* 2011; Stoker *et al.*

2018). This architecture reflects the long-term persistence of the Rona Ridge as an emergent topographic high from Triassic to Cretaceous times. Regional subsidence and burial occurred in the Late Cretaceous, blanketing the ridge in deep marine mudstones that are thought to form the regional seal (Ritchie *et al.* 2011; Witt *et al.* 2011; Trice 2014). Most cores of the basement–cover unconformity reveal little evidence of deep surface weathering of the exposed crystalline rocks, unlike other basement plays such as the Utsira High in the Norwegian North Sea (Riber *et al.* 2017; Trice *et al.* 2019). Thus, most of the basement-hosted oil in the Rona Ridge is probably hosted in fractures (Holdsworth *et al.* 2019).

The Lancaster field

Exploration and appraisal

The Lancaster basement was first drilled in 1974 by Shell in well 205/21-1a to evaluate a Mesozoic clastic succession (Jurassic Rona Sandstone) that onlapped the basement (Fig. 1c). Oil was recovered to surface with core samples revealing oil associated with fractures in both the Rona Sandstones and the underlying basement.

Subsequently five basement exploration–appraisal wells were planned and drilled based on the interpretation of 3D seismic reflection data and the identification of faults extending down into the basement (Figs 1c and 2a). Each of the Lancaster wells has undergone drill stem testing and the associated dynamic data combined with interpretation of wireline or logging while drilling (LWD) logs, core and sidewall cores have led to the current understanding of the Lancaster reservoir (Fig. 3; see Slightam 2012; Trice 2014; Belaidi *et al.* 2016; Bonter *et al.* 2018; Trice *et al.* 2019). The Lancaster field is currently under production through two, 1 km long, horizontal wells, which are tied back to a floating production, storage and offtake vessel. Initial production achieved individual well flow rates of 16 500 bopd and an extremely high productivity index of between 190 and 205 STB/d/psi. The latter is consistent with an extensive oil column (estimated range of 597–678 m TVT) and a well-connected hydrodynamic fracture network.

The geological history and reservoir characteristics of Lancaster indicate that the trap is a 'buried hill' similar to other global examples such as the Bach Ho Field in Vietnam (Cuong & Warren 2009; Trice *et al.* 2019). The current exploration model suggests that the Lancaster field and the adjoining Halifax discovery are part of a single hydrocarbon accumulation, with the trap sealed by overlying and draping Cretaceous mud rocks and perhaps laterally by the Westray Fault Zone and Brynhild Fault Zone (Fig. 2b).

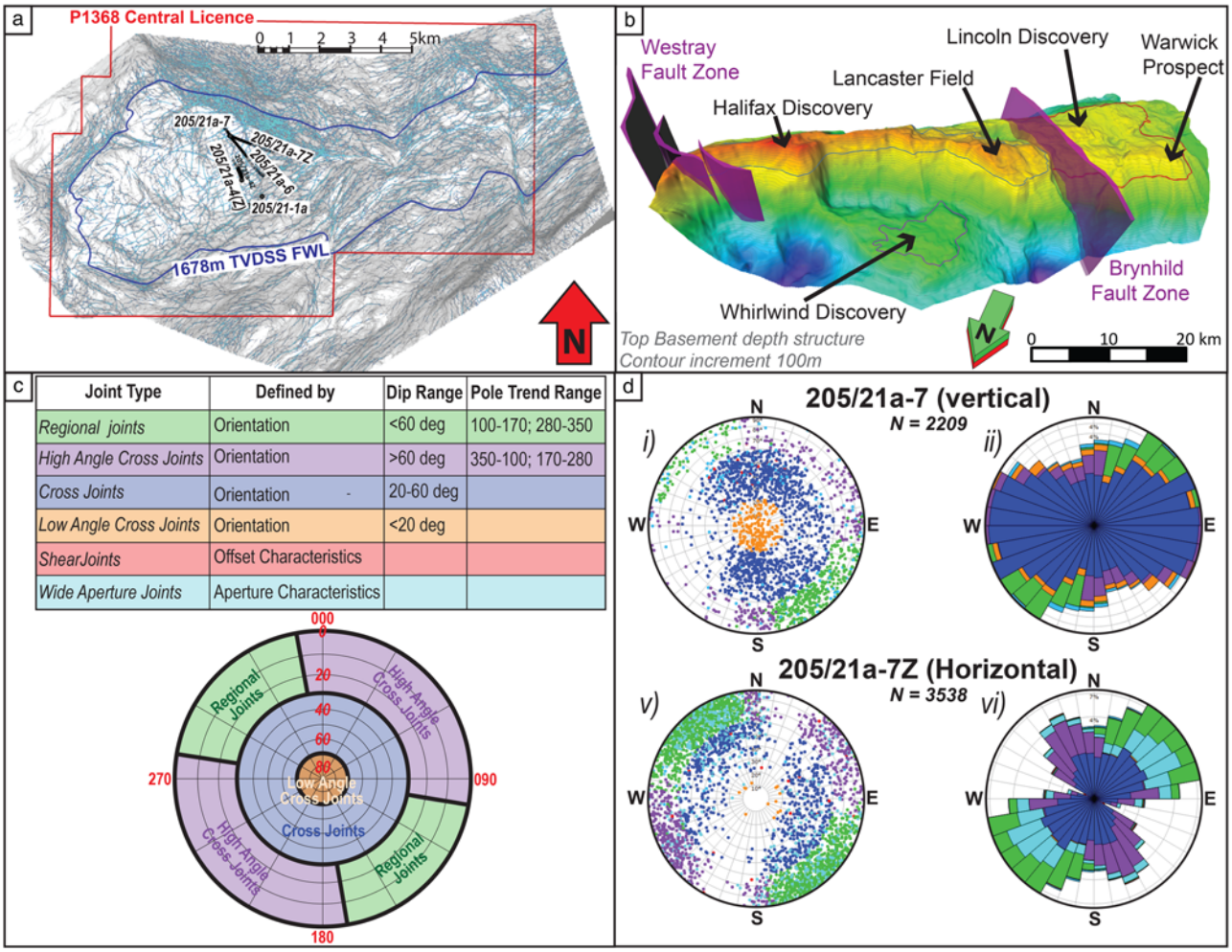

Fig. 2. (**a**) Seismic fault map at top basement for the Lancaster field showing location of main legacy, exploration and appraisal wells. Faults denoted as blue and grey lineaments are automatically picked from the uppermost 10 ms of the seismic volume utilizing coherency analysis (Antracking©) with parameters constrained by manual seismic interpretation and well data. Antracking is a product of Schlumberger and forms part of the Petrel suite of programs. TVDSS FWL, true vertical depth sub-sea free water level. (**b**) Three-dimensional oblique view looking SE of top basement surface showing location of Lancaster field relative to adjacent discoveries and prospects in the SW Rona Ridge. The location of the NW–SE Westray and Brynhild fault zones is also shown. (**c**) Lancaster joint classification scheme used by Belaidi *et al.* (2016). (**d**) Schmidt upper hemisphere polar plot (left) and rose diagram (right) for joints identified from image logs in the basement wells 205/21a-7 (vertical 1397 ft (425.8 m) MD) and 205/21a-7Z (horizontal 3226 ft (983.3 m) MD). It should be noted that the Wide Aperture Joints (light blue) show a preferential distribution similar to that of the NE–SW Regional Joints (green).

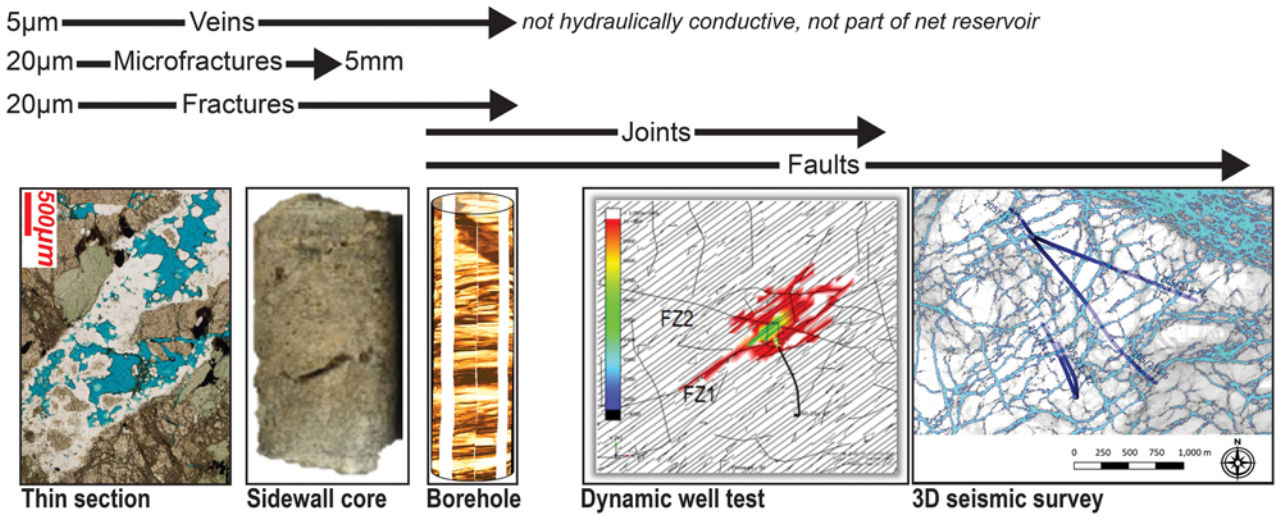

Fig. 3. The scales and classification scheme of fractures used for the Lancaster basement by Belaidi *et al.* (2016) and Bonter *et al.* (2018) and the range of data types used to image and understand these fractures.

Fracture network characteristics from wireline or LWD, image log data and cores

The Lancaster area has good 3D seismic data coverage of reasonable quality allowing faults penetrating top basement to a depth of at least 150 m to be identified with confidence (Fig. 1c; Slightam 2012). These have been mapped out across the top basement surface (Fig. 2a) using automatic picking in the uppermost 10 ms of the seismic volume utilizing coherency analysis, the parameters of which were constrained based on manual interpretation of seismic and well data.

All seismically mapped basement faults intersected by Lancaster wells drilled to date have been demonstrably porous and permeable (e.g. Belaidi *et al.* 2016; Bonter *et al.* 2018). The associated fracture network appears to form a deeply penetrating and well-connected fissure system (Slightam 2012; Trice 2014). Belaidi *et al.* (2016) subdivided the network into scale-dependant fracture types referred to as 'microfractures', 'fractures', 'joints' and 'faults' (Fig. 3); they also identified 'veins', which were taken to be fractures completely occluded by impermeable mineral fills. 'Microfractures' (and veins) were identified and characterized from sidewall cores using petrophysical measurements, 3D scanning techniques for porosity and density, and preliminary thin-section analysis. The term 'fracture' was used to describe lineaments with observable trace lengths longer than the sampling medium, be it thin section, core or borehole diameter. Thin-section analysis of the cores indicates that minimum effective microfracture and fracture apertures are 20 μm (Belaidi *et al.* 2016). The majority of Lancaster cores are acquired through the process of rotary sidewall coring, all of which exhibit natural fractures. This observation is testament to the high fracture frequency of the Lewisian basement as the sidewall cores were targeted to minimize the presence of fractures so as to optimize core recovery.

Fractures that cut an entire borehole and are identified from borehole image logs are referred to as 'joints'. These can be subdivided into classes based on orientation and apparent aperture width (Fig. 2c; Belaidi *et al.* 2016). Of these classes, 'Regional Joints' show a distinct Mesozoic NE–SW trend parallel to the strike of the Rona Ridge (Fig. 2d) and are more typically associated with higher measured porosity (Bonter *et al.* 2018) and wider apparent apertures. The 'Wide Aperture Joints' share a predominantly NE–SW trend (Fig. 2d), exhibiting apparent apertures in excess of 2 cm (Belaidi *et al.* 2016) meaning that they are particularly important when evaluating the dynamic properties of the reservoir and its long-term production potential. 'Faults' are identified from 3D seismic data (Fig. 3; Slightam 2012; Belaidi *et al.* 2016) and are associated with zones of fractured rock that have enhanced reservoir properties compared with the background fractured basement. On average, these zones are interpreted as being *c.* 40 m wide and have been identified through the interpretation of drilling and wireline or LWD logging data.

Basement reservoirs developed in crystalline rocks with igneous plutonic protoliths like those in Lancaster (see below) tend to be associated with the development of non-stratabound joint sets (Koenders & Petford 2003). These tend to show depth-invariant frequencies (intensities) that can extend to depths of a kilometre in the crust (Seeburger & Zoback 1982). The Lancaster joints seen in image logs exhibit constant intensity regardless of proximity to faults, fault zones and top basement and also with depth (Trice *et al.* 2019). This is consistent with the presence of an early and pervasive set of cooling joints, which were then exploited by subsequent faulting and fissuring in a manner similar to that observed along reactivated joint sets in the brittle-deformed parts of the Adamello massif in the Italian Alps (Dempsey *et al.* 2014). Fault aperture distributions measured on image logs from wells 205/21a-4 and 205/21a-4Z display a power-law relationship with a low scaling exponent (alpha ~ 0.6; Fig. 4a), indicating that there are more wider aperture structures relative to narrow structures compared with typical fracture aperture distributions (e.g. Bonnet *et al.* 2001). We propose that this observation is consistent with the development of fissure-type structures developed on the Rona Ridge (Trice *et al.* 2018, 2019; Holdsworth *et al.* 2019; McCaffrey *et al.* in preparation).

The relationship of joints to faults is important as there is strong evidence through topological analysis that a highly connected fault network exists within the Lancaster reservoir. We followed the method of Sanderson & Nixon (2015) by defining fracture nodes and branches on Lancaster fault maps (Fig. 4b). The four topology analyses performed show the nodal ratios plotted relative to other studies on the Rona Ridge and onshore Lewisian reported by McCaffrey *et al.* (in preparation) (Fig. 4b). The Lancaster analysis shows highly connected fault topologies with connection per branch (C_B) values $\gg 1$ (the threshold C_B for a connected network). Most outcrop and core samples from the onshore and offshore basement show a predominance of Y node-dominated fracture networks (Fig. 4b), also meaning high connectivity. The high connectivity of the fault and joint networks in Lancaster is reflected by the production data, which describe a well-connected fracture system and associated high productivity index for the wells (RPS 2017).

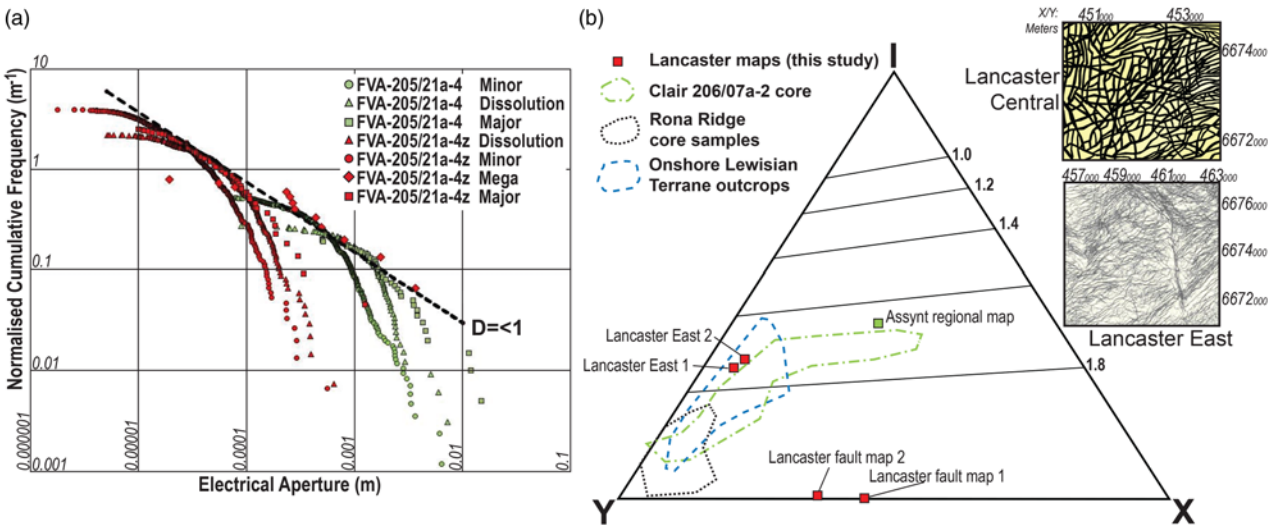

Fig. 4. Fracture attribute data for the Lancaster field. (**a**) Fracture intensity (cumulative number normalized per metre) v. aperture for wells 205/21a-4 (green) and 205/21a-4Z (red). Data derived from measurements made using well image logs. (**b**) Ternary diagram plot of node types. I-type is where a fracture terminates against another; Y-type is where a fracture abuts against or splays from another; X-type is where fractures intersect one another. Contours are of C_B (connections per branch), with 1.0 being the threshold for connectivity. Images of the fault maps used for the study are shown to the right (details of how these were derived have been given by Slightam 2012).

Sidewall core descriptions

Sidewall cores were preferentially taken from volumes of rock that exhibit the least fracturing as detected from electrical image logs to optimize core recovery. The location of sidewall cores in both depth and azimuthal position in the borehole wall was confirmed post core acquisition by the use of acoustic image logs, particularly transit time images (Belaidi *et al.* 2016). Despite the applied sampling strategy, the majority of acquired sidewall cores from Lancaster contain natural fractures, some of which are associated with mobile oil.

The present paper focuses on cores taken from wells 205/21a-4Z, 205/21a-7 and 205/21-1A (Fig. 2a); all cores cited in this paper are referred to using measured depths (MD). The basement rocks are unconformably overlain by a range of thin (5–35 m thick) carbonate-cemented sandstones of different ages: Jurassic Rona Sst in 205/21-1A, Lower Cretaceous Victory Formation in 205/21a-7 and Upper Cretaceous Commodore Formation in 205/21a-4Z. In all cases, these local cover sequences are in turn overlain by thick sequences of younger Cretaceous shales and thin carbonates.

In the legacy core from 205/21-1A, top basement is at 4439 ft (1353 m), with tonalitic basement cored 15 m down to 4488 ft (1368 m). Top basement is at 4033 ft (1229.3 m) in 205/21a-4Z with 21 sidewall cores collected over an interval of just less than 50 m from depths of 4605–5065 ft (1404–1544 m). These are predominantly tonalitic in composition, with a thick composite sheet of mafic dolerite recognized between 4926.5 and 5011 ft (1502–1527 m). Slightam (2012) has reported a K–Ar age of *c.* 2300 Ma from this unit. In Well 205/21a-7, top basement is located at 4512 ft (1375.5 m), with 64 sidewall cores sampling predominantly tonalitic rocks over a 450 m long interval from depths of 4541–5919 ft (1384–1804.5) m.

The following sections summarize the main lithologies and textures of the basement host rocks seen in legacy cores held by the BGS at Keyworth (205/21-1A) or in the Hurricane sidewall cores (205/21a-4Z, 205/21a-7), followed by a description of the fault rocks and fracture fills. All thin sections are impregnated to reveal porosity (blue) and stained to reveal calcite (pink) and K-feldspar (yellow). Samples from the three wells are for the most part very similar and so are described together, although any important differences are highlighted. In 205/21a-7, several sidewall cores were collected in the uppermost 15 m of basement close to the top basement unconformity. These reveal a thin (*c.* 15 m thick) zone of more weathered basement material compared with the relatively fresh metamorphic rock that makes up much of the remaining wells. The Rona Sandstone–basement contact is preserved in 205/21-1A with little sign of weathering, although a coarse basal conglomerate–breccia unit *c.* 5 m thick contains numerous sub-angular to rounded blocks of tonalitic basement. No sidewall samples were collected close to the unconformity in 205/21a-4Z, so it is unknown if a weathered zone is present here. Deep weathering below the top basement unconformity is generally not seen along the Rona Ridge (Holdsworth *et al.* 2019), although extensive alteration is seen along deeply penetrating fissures that connect to the palaeosurface.

Host rocks

The overwhelming majority of basement rocks are pale grey–green coarse-grained metatonalites (Fig. 5a and b) composed of plagioclase, quartz, orthopyroxene (hypersthene) ± hornblende, clinopyroxene (augite), secondary biotite, K-feldspar and accessories (apatite, titanite, ore, zircon). The rocks are generally very weakly foliated, with only poorly developed local compositional layering on centimetre scales. Finite strains are low, but primary igneous textures (such as poikilitic textures, compositional zoning and intergrowths) are not preserved in thin section. Instead, the widespread development of tapered twinning in plagioclase and seriate–interlobate to amoeboid textures for plagioclase–quartz grain boundaries (Fig. 5c) point to the operation of grain boundary migration recrystallization under at least amphibolite-facies metamorphic conditions (Passchier & Trouw 2005). The ubiquitous development of orthopyroxene assemblages is, however, consistent with granulite-facies metamorphism, meaning that these rocks are charnockites (Frost & Frost 2008). This is significant for the later development of Lancaster as basement rocks of this type and composition are known to be mechanically strong and highly resistant to weathering, even in tropical environments (e.g. Gunnell & Louchet 2000).

The large mafic sheet in 205/21a-4Z comprises a 13 m thick unit of medium-grained dolerite with phenocrysts of augite and olivine set in a finer matrix of augite, olivine, brown hornblende, biotite and ore (Fe oxide, pyrite) (Fig. 5d). Both plagioclase and Fe-dolomite are present as interstitial phases. The olivine and Fe oxide are

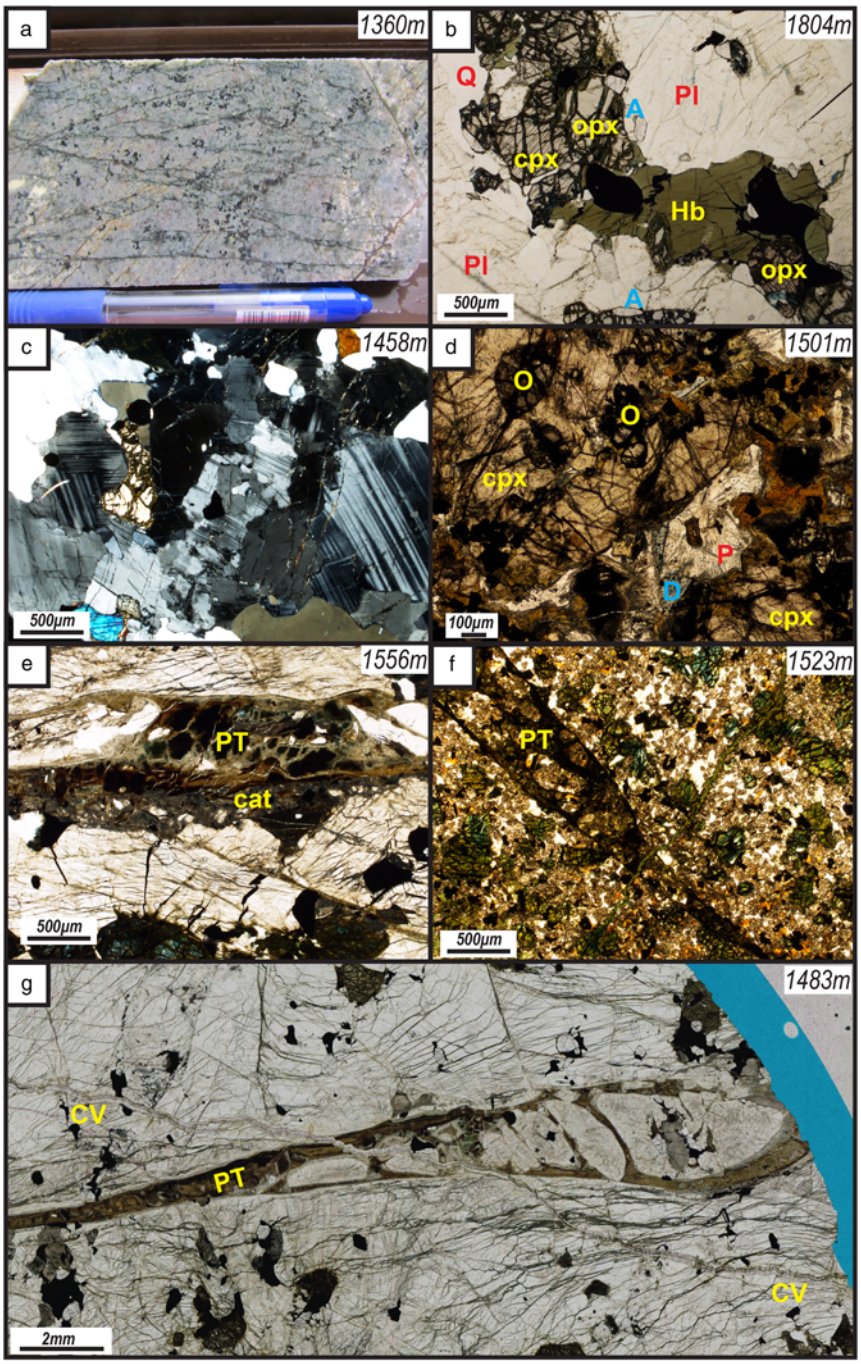

Fig. 5. Composition, textures and early deformation of the Lancaster basement. (**a**) View of typical grey metatonalite showing weak foliation and conjugate microfractures. (**b**) Plane-polarized light (PPL) thin-section view of little altered metatonalite showing plagioclase (Pl), quartz (Q), orthopyroxene (opx; hypersthene), hornblende (Hb), clinopyroxene (cpx; augite) with accessory apatite (A) and ore (black). (**c**) Cross-polars thin-section view of typical tapered twinning and minor recrystallization in plagioclase and seriate–interlobate to amoeboid textures for plagioclase–quartz grain boundaries. (**d**) PPL view of dolerite showing small rounded, partially altered olivines (O) poikilitically enclosed by large clinopyroxene (cpx; augite) grains with rims of green–brown amphibole. Interstitial form of plagioclase (P), with radiating needles of apatite–clinozoisite and blue-stained dolomite (D), should be noted. (**e**) Grey chlorite–quartz cemented cataclasite seam (cat) cutting fractures and partially altered metatonalite overlain by composite brown–green altered pseudotachylyte (PT), which is itself locally re-brecciated during multiple shearing events. (**f**) Finer grained dolerite cross-cut by altered pseudotachylyte (PT) vein with rounded wall rock clasts; it should be noted that this is cross-cut by later green clay-filled microvein. (**g**) Low-power PPL view of brown pseudotachylyte vein with rounded wall rock clasts cutting fractured metatonalite; cross-cutting sinuous vein of fibrous calcite (CV) should be noted. Images are from the following well cores: 205/21-1A (**a**), 205/21a-7 (**b**, **c**, **e**, **g**) and 205/21a-4Z (**d**, **f**).

texturally early, being widely enclosed by augite. Olivine is locally altered to serpentinite, and together with augite is widely rimmed by brown–green hornblende and later tremolitic alteration rims. Both plagioclase and Fe-dolomite contain radiating needles of apatite and sheaves of zoisite–clinozoisite. Magmatic and solid-state deformation fabrics are entirely absent in the dolerites, although they are cut by fractures (see below).

Early brittle deformation and associated retrogression

Heterogeneously developed sets of microcracks are seen in most sidewall cores of the charnockitic basement, together with shear fractures, cataclasites and pseudotachylytes. All are cross-cut and locally reactivated by the later fractures, veins and fissure fills described in the following section.

The microcrack arrays and shear fractures occur typically in subparallel sets or less commonly as conjugate sets. The cracks are variously filled with hematite, limonite, sericite, fine epidote or quartz (e.g. Fig. 5e), with the last growing in optical continuity with host quartz grains forming healed crack arrays. Partial or complete alteration of mafic minerals, especially hypersthene to fine-grained aggregates of uralite, talc, carbonate, epidote, biotite, chlorite and hematite, is widespread (Fig. 5e and f), as is the patchy alteration of plagioclase to sericite. More extensive seams of cataclasite up to 5 mm thick are widespread with quartz–chlorite cements (Fig. 5e). Thin, continuous anastomosing and coalescing veins of brown–green altered pseudotachylyte up to 1 mm thick are found in several samples from 205/21a-7 and are consistently associated with zones of slightly earlier cataclasis (Fig. 5e and g). These locally display tapering injection veins, rounding of wall rock clasts and complex flow banding, with marginal haloes of clay or cryptocrystalline silica or quartz. Incipient breccias and sidewall rip-outs are locally developed. Offset grains and secondary Riedel shear arrays are widely associated with shear fractures, cataclasites and pseudotachylytes and are always kinematically consistent with one another, suggesting that these features are at least locally the same age. In a

few cases, however, pseudotachylytes are brecciated by later cataclasis (e.g. Fig. 5e) suggesting multiple slip events. Cataclastic shear fractures, some of which are associated with talc mineralization, and possible veins of altered pseudotachylyte also cut the dolerite sheet in 205/21a-4Z (Fig. 5f).

Thin (<1 mm thick) sinuous and anastomosing veins of chlorite + quartz ± epidote, albite, zeolite and rare calcite are sparingly present in all three wells cross-cutting all of the above features. They appear to represent a distinct and younger phase of mineralization that predates the predominant younger set of mineral and hydrocarbon-bearing fracture fills.

Later hydrocarbon-bearing mineralized fissure fills and fractures

These features cross-cut or reactivate all earlier features described above. Tensile or hybrid fracture modes dominate, with only small-offset shear fractures (<2 mm displacement) developed locally. The fractures are variously filled with a diverse range of mineral cements, with no consistent order of mineralization or deposition seen even within individual samples. Larger fissures additionally contain fine- to very coarse-grained clastic sediment fills, some with depositional laminae.

The most heavily oil-stained features are fissure fills that range in thickness from <1 mm to >0.5 m, all of which are characterized by the presence of clastic material in addition to mineral fills (Fig. 6a–f). Belaidi *et al.* (2016) have suggested that these may reach widths of 2 m or more. Grouped fractures of this kind could result in amalgamated apertures extending up to several tens of metres. Numerous small (<1 cm wide) and several large (>0.4 m wide) fissures and associated mineral veins are sampled in sidewall cores from 205/21a-4Z (e.g. 4771 ft (1363 m) and 4957 ft (1511 m) hosted in dolerite; 5035–45 ft (1535–8 m)) and 205/21a-7 (e.g. 1989–90 m, 1475–80 m and 1550–62 m). These are highly diverse in terms of both their mineral fills and textures, but show a number of features in common.

Typically fissure fills are composite features that preserve evidence of multiple phases of opening, mineralization and filling (e.g. Fig. 6a–f). They are characterized by the presence of numerous angular to sub-angular brecciated clasts of both altered wall rock and earlier mineral or sediment fills (Fig. 6b–d). Clasts are chaotically distributed and show little evidence for abrasion. A crude alignment of clasts and fills may occur parallel to the fissure margins (Fig. 6c–e) and appears to be a result of compaction acting across the fissures rather than shear.

Some fissure fills run subparallel to earlier zones of cataclasite and pseudotachylyte (e.g. Fig. 6d), which may have therefore been

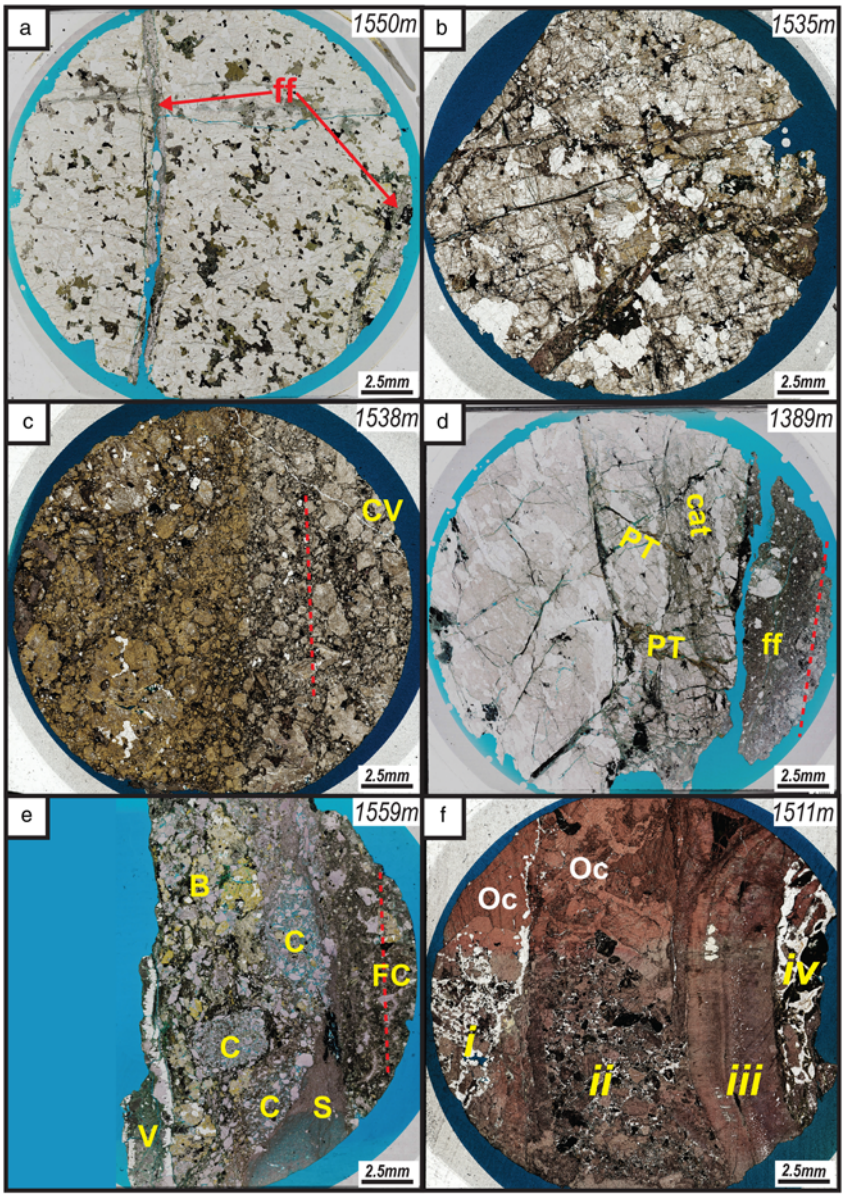

Fig. 6. Low-power thin-section views of fissure fill development at different stages in 2 cm diameter sidewall cores (see also Fig. 7a–h). (**a**) Two narrow (<2 mm wide), subparallel fissure fills (ff) cutting otherwise intact, weakly foliated metatonalite. (**b**) Fissure fill comprising mainly highly fractured angular clasts of wall rock forming a jigsaw-type breccia with calcite–clay–K-feldspar–albite–pyrite cemented matrix filling and fracture fills. (**c**) Clastic breccia fill (sample stained only on LH side) with K-feldspar altered wall-rock clasts set in a red–brown clay-rich matrix locally cemented by carbonate (pink); crude foliation defined by vertical alignment of clasts (red dashed line) and sinuous cross-cutting calcite microvein (CV) should be noted. (**d**) Fissure margin showing early subparallel pale grey cataclasites (cat) with associated brown pseudotachylytes (PT) in wall rock cross-cut by later oil-stained carbonate–clay cemented breccia fill (ff) with margin-parallel foliation (red dashed line). (**e**) Oil-stained composite fissure fill including clast-supported K-feldspar altered breccia (B), porous breccias rich in calcite clasts (C), fine sediment fill (S), composite quartz–calcite–green clay vein (V) and radial fibrous calcite cemented breccia (FC). Crude vertical foliation in later subparallel to composite vein should be noted. (**f**) Dolerite cross-cut by complex mineralized fissure fill with at least four different fill sets, all of which are oil-stained: (i) rounded altered clasts of dolerite and calcite with vuggy quartz–chalcedony fills partially occluded later Fe-calcite fill (Oc = geopetal feature?); (ii) cockade-style quartz and calcite cements with rounded clasts of altered dolerite and early calcite again occluded at one end by later calcite fill (OC) as in zone (i); (iii) fibrous calcite vein with intergrown subordinate silica (quartzine–chalcedony); (iv) like zone (ii), with altered dolerite and calcite clasts with oil-stained patches of colloform chalcedony. Zones (i) and (iv) may be part of the same fill and oldest. Images are from the following well cores: 205/21a-7 (**a**, **d**, **e**) and 205/21a-4Z (**b**, **c**, **f**).

reactivated by tensile fracture opening. In other cases these features are cross-cut by fissures at a variety of angles. Some fills are little more than zones of jigsaw-brecciated wall rocks (Fig. 6b) whereas others contain a diverse range of materials that are very different from the immediate wall rocks (e.g. Fig. 6e). Crudely laminated and graded sediments are present locally in some larger fills (Fig. 7a). Fissure or fracture margins and wall rock clasts are commonly lined by fine clay formed immediately prior to partial to near-complete infilling by a diverse range of mineral cements including calcite, Fe-calcite, clays (green smectites and brown illite), K-feldspar, pyrite, iron oxides, quartz and micro- or crypto-crystalline silica (including chalcedony) (Fig. 7a–h). These are commonly intergrown with colloidal textured clays where crystallization has occurred synchronously with calcite or quartz or silica (Fig. 7c).

Wall rocks, fills and wall rock clasts are typically cut by numerous arrays of microcracks and shear fractures with vuggy composite mineral fills that are sometimes the same as or different from those that cement the adjacent fissure fills (e.g. Fig. 7b). Many fissure fills also include locally later composite veins up to 2 cm thick that run subparallel to the fissure margins (Fig. 6d and e). The mineral fills in these veins are commonly diverse and in some cases carry 'exotic' mineral cements such as clinozoisite or zeolite.

Vuggy mineral textures are particularly associated with quartz and K-feldspar veins or cements (Fig. 7a, b, d and e) and vugs may either be preserved as open pores or be occluded by locally later fills such as calcite, clay or oil. Some of the larger fissure fills are characterized by visible porosity values in excess of 10% (e.g. Fig. 7a, d and e). The widespread preservation of cockade style, rind and concentric mineralization textures (e.g. Fig. 7c, f and g) suggests an epithermal style of hydrothermal mineralization in long-lived, partially open near-surface fractures. Fibrous mineral fills are subordinate features and seem most widespread when clays are also present. A characteristic feature is that wall rock grain compositions locally control fracture fill mineralization via overgrowth development, particularly for quartz, feldspar and clays (Fig. 7e). Hydrocarbon (bitumen) is associated widely with both mineral and sediment fills occurring as fluid inclusions in minerals (calcite, clay, quartz–silica), pores, vugs and fractures.

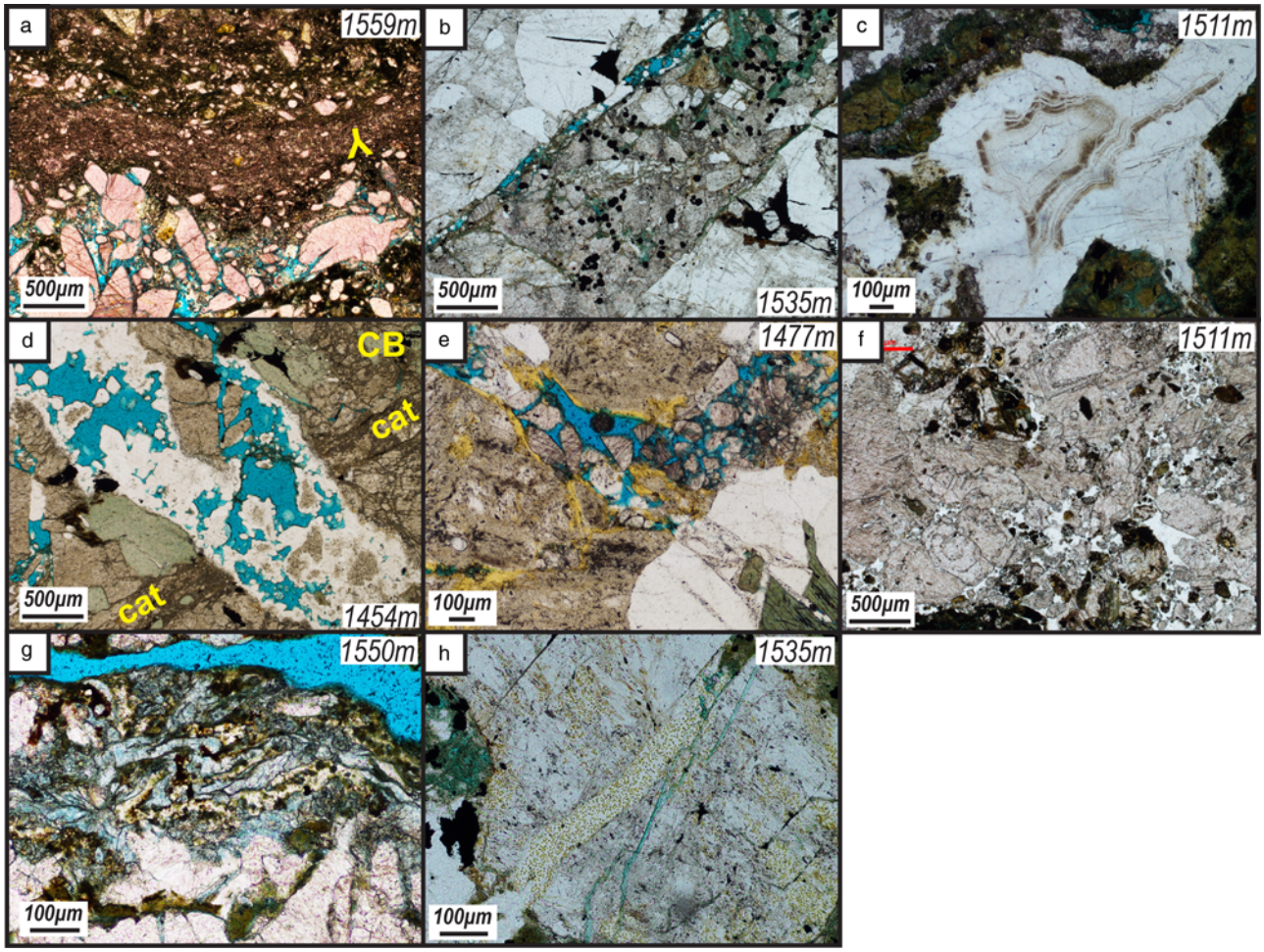

Fig. 7. Fissure fills and associated hydrothermal mineral fills from Lancaster stained thin sections (all views PPL). (**a**) Lower part shows highly porous carbonate (pink stain) clast breccia overlain by younger laminated oil-stained sediment with possibly graded bedding (from fill shown in Fig. 6e). Younging direction shown by inverted Y. (**b**) Calcite–clay–K-feldspar (yellow stain)–albite–pyrite cemented fissure fill with clay-lined walls cut by margin-parallel vuggy quartz–K-feldspar filled fracture (at top) (from fill shown in Fig. 6b). (**c**) Colloform oil-stained chalcedony intergrown with dark colloform clays (from fill set (iii) shown in Fig. 6f). (**d**) Vuggy quartz (overgrowing host quartz)–cryptocrystalline silica (overgrowing feldspar) fill cutting earlier cataclasite seam (cat) and calcite-cemented breccia fill (CB). (**e**) Vuggy quartz–K-feldspar fracture cross-cutting earlier K-feldspar-altered breccia fill. Almost complete healing of microfracture in host quartz grain with mineral and oil inclusions should be noted. The rounded appearance of the calcites in the fracture fill has been taken by Belaidi *et al.* (2016) as evidence for dissolution processes prior to ingress of oil. (**f**) Quartz–silica cemented breccia with clasts of altered dolerite (dark) and multiply zoned calcite showing cockade-style textures (from fill shown in Fig. 6f). (**g**) Stacked 'bacon-rind'-like overgrowths of Fe-calcite (bluish stain) and chalcedony–clay on clasts and walls in fissure fill. (**h**) Colloform 'moss' texture of yellow-stained K-feldspar (with each grain <5 μm across) surrounded by albite overgrowing areas of antiperthite and healed microfracture in host feldspar grain (from fill shown in Fig. 6b). Images are from the following well cores: 205/21a-7 (**a**, **e**, **g**) and 205/21a-4Z (**b–d**, **f**, **h**).

Wall rocks adjacent to fissures and included wall rock clasts show widespread evidence of fluid-related replacement with feldspars altered to sericite and K-feldspar, and mafic minerals altered to clays. In all of 205/21a-4Z and the upper parts of 205/21a-7 close to the weathered zone and within larger fissures at greater depth, K-feldspars show a characteristic fine colloidal or moss-like growth form (Fig. 7h) both in host feldspar grains, where they grow over primary regions of antiperthite, and in fractures, where they are enclosed in secondary albite that grows in optical continuity with wall rock or clast plagioclase. Although quartz mineralization is widespread, some fissure fills and composite veins also carry extensive regions of cryptocrystalline silica or banded chalcedony, both of which may be intergrown with other minerals including colloidal clay and fine disseminated calcite (Fig. 7c and g).

Oil-bearing fissure networks dominated by sediment and vuggy calcite fills are widely developed in both the basement and well-cemented Jurassic Rona Sandstone cover rocks in well 205/21-1A (Fig. 8a–c). Filled fractures with fine depositional laminations are preserved locally and consistently young up the core (Fig. 8c). Basement-rooted fractures are also inferred to cut the Victory Formation sandstones in 205/21a-7 as significant mud losses were encountered in this unit during drilling of 205/21a-6, 205/21a-7 and 205/21a-7Z (C. Slightam. pers. comm., 2019). Similar subterranean cavity fills are seen in basement fractures elsewhere along the Rona Ridge (Holdsworth *et al.* 2019).

The identification of fissures, and their associated fills, provides a geological mechanism to account for the generation and preservation of the 'Wide Aperture Joints' identified from the image logs and production logging tools (e.g. Fig. 9a and b). These features are demonstrably associated with oil production and are therefore interpreted as representing examples of (buried) permeable fissures.

The weathered basement of 205/21a-7

The uppermost 10–15 m of the basement immediately below the erosional unconformity with the Lower Cretaceous Victory Formation has a greenish hue in hand specimen. In thin section, it shows pervasive clay-filled microfracturing and near-total alteration of mafic minerals to clay (Fig. 10a and b). Significant porosity (up to 10%) is seen in fracture fills and altered or fractured primary minerals, with millimetre to centimetre thick sediment and mineral-filled fissure development widespread; open fractures <5 μm wide are also preserved (Fig. 10a). Oil stains and local bitumen fills are common. The mineral fills of calcite, clays (brown illites, green smectites), K-feldspar, zeolite, pyrite, Fe oxides and, less commonly, silica (quartz, cryptocrystalline silica) are identical to those seen associated with the main phase of hydrocarbon-bearing fractures in the deeper basement. The preservation in the weathered zone of cockade and vuggy mineral textures confirms this similarity, implying that the processes of fracturing, fissure formation, hydrothermal mineralization, fluid-related alteration of fills and weathering all occurred broadly contemporaneously in fractures located at or connected to the near surface. The preserved geological relationships suggest that this occurred at some time after the deposition of the Jurassic Rona Sandstone (as seen in 205/21-1A) and that it at least began prior to deposition of the Upper Cretaceous Victory Formation (as seen in 205/21a-4Z).

U–Pb zircon dating of host basement rocks

Three core samples of weakly deformed charnockitic tonalites from 205/21a-7 (at 1389.8, 1543.0 and 1697.4 m) were submitted for zircon U–Pb isotopic analysis, to provide constraints on the age of the basement rocks in the area. Analytical methods are discussed in Supplementary material Table I, and the U–Pb isotopic compositions and ages are given in Supplementary material Table II.

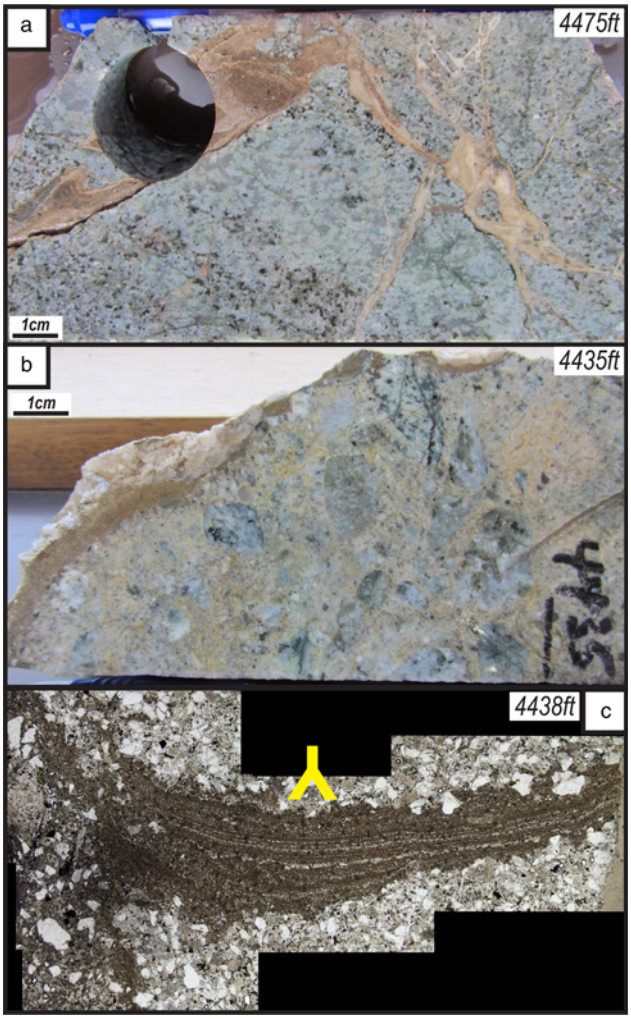

Fig. 8. Sediment-filled fractures from legacy well 205/21-1A. (**a**) Laminated sediment and carbonate mineral fills in fractured or fissured metatonalitic basement; (**b**) oil-stained sediment–sparry calcite fill in fracture (top) cutting paler well-cemented Rona Sandstone cover sequence breccia; (**c**) PPL view thin-section montage of laminated sediment with grading giving way up, filling triangular fissure in carbonate-cemented low-porosity Rona Sandstone.The total horizontal distance across the bottom of 8c is 20 mm.

Zircon habits in all three samples range from equant to elongate prismatic with indistinct oscillatory magmatic zoning (Fig. 11ai–ci). They are mostly dark under CL (high-U), with some grains having bright (low-U) rims, whereas a small number are entirely bright under CL. On Wetherill concordia diagrams (Fig. 11aii), the zircons in the 1389.8 m sample display a discordant trend with an upper intercept age of 2743 ± 10 Ma with an MSWD of 0.55. A concordia age of 2743 ± 6 Ma, virtually identical to the upper intercept age, can be determined on the basis of zircons with 99–101% concordance (Fig. 11aii). In the 1543.0 m sample, the majority of zircons plot on or close to the concordia line. The group of 22 zircons with 99–101% concordance, excluding three older, potentially inherited, grains yield a concordia age of 2736 ± 7 Ma with an MSWD of 0.4 (Fig. 11bii). In the 1679.4 m sample, virtually all zircons plot on or close to the concordia line with only one older grain interpreted as inherited (Fig. 11cii). The 31 zircons with 99–101% concordance, excluding the inherited grain, yield a concordia age of 2731 ± 6 Ma with an MSWD of 0.76 (Fig. 11cii).

In the 1679.4 m sample, there is a distinct difference in age between the darker-luminescing cores and the bright rims (Fig. 11ci). This gives rise to a bimodal distribution on a probability density plot (Fig. 11ciii), with a main peak in the 2730–2760 Ma

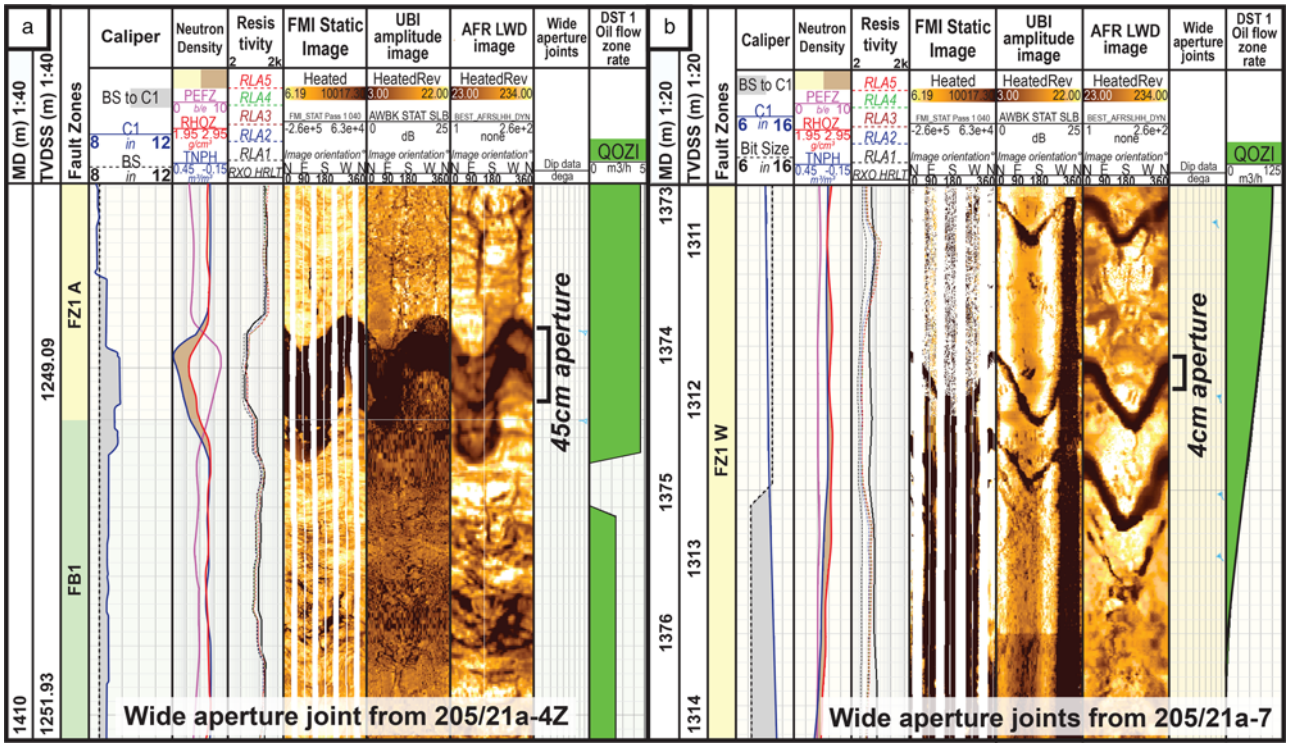

Fig. 9. Log data from (**a**) 205/21a-4Z and (**b**) 205/21a-7 across intervals of fractured basement (FB) and interpreted fault zones (FZ). Locations of 'Wide Aperture Joints' estimated at 45 and 4 cm are indicated.

range and a subsidiary peak between 2700 and 2710 Ma. In the other two samples, the ages of cores and rims are within error of each other and virtually all the zircons form a single peak on the probability density plot (Fig. 11aiii and biii). However, both samples contain isolated younger zircons yielding ages around *c.* 2700 Ma. In the 1543.0 m sample, a slightly older group of zircons between 2770 and 2790 Ma may be xenocrystic, as may a single older zircon in the 1697.4 m sample.

Collectively, the three samples yield very similar concordia ages in the range 2743–2731 Ma, all of which overlap within error; this is interpreted as the primary crystallization age of the zircons. The subsidiary group of younger ages (*c.* 2700–2710 Ma) obtained from rims in the 1679.4 m sample and isolated zircons from the other two samples are interpreted to represent a younger metamorphic or anatexis event at this time, whereas the small group of older zircons in the age range *c.* 2770–2790 Ma are interpreted to be xenocrystic.

U–Pb dating of calcite vein fill

Geochemical analysis of five calcite fracture fills was undertaken at the University of Hull using *in situ* laser ablation inductively coupled mass spectrometry (LA-ICP-MS), as described in Supplementary material Table III. One calcite fill sample, A57

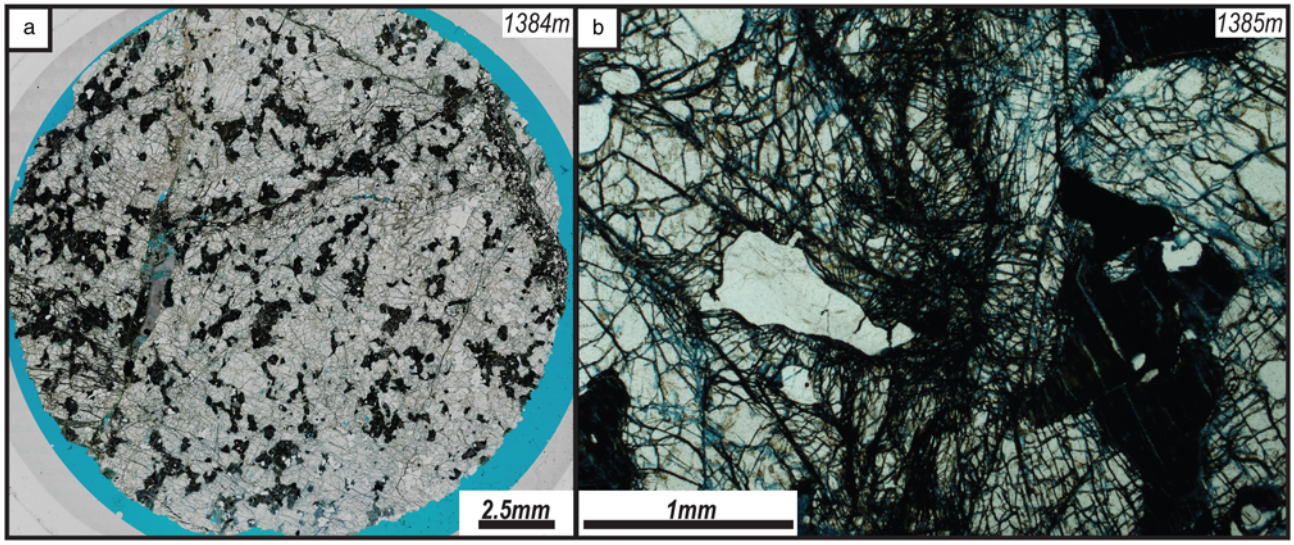

Fig. 10. Weathered basement from Lancaster well 205/21a-7. (**a**) Low-power PPL view of 2 cm diameter core with porous, vuggy fissure fills partially filled with calcite and sediment, with extensive clay-lined microfracturing of host basement rock. (**b**) Close-up PPL view showing almost complete alteration of mafic minerals to dark clays identical to those filling the microfractures; the fracturing is noted mainly by the feldspars and largely bypasses the quartz grains. Both images from the weathered section in 205/21a-7.

(1744 m, well 205/21a-7; Fig. 12a), was found to contain appreciable amounts of uranium and was thus suitable for U–Pb dating (Fig. 12b). The fracture fill comprises a single monomineralic calcite vein <4 mm thick, which is itself cross-cut and offset by a narrow <1 mm polymineralic vein (iron oxide, clay and minor uranium-poor calcite). A total of 348 spots were analysed from the sample, yielding a calcite U–Pb date of 108.73 ± 0.83 Ma, MSWD = 1.7 (Fig. 12c).

Discussion

Affiliation and significance of the Lancaster basement

The *c.* 2743–2731 Ma U–Pb zircon ages from the three basement well samples dated fall in the centre of the range of Neoarchean ages (2700–2829 Ma) obtained by Chambers *et al.* (2005) and Holdsworth *et al.* (2018) from basement orthogneisses found in 20 borehole cores covering a wide offshore region north of Scotland and west of Shetland. More recently, Kinny *et al.* (2019) have obtained an almost identical set of ages (2746–2726 Ma) onshore from seven samples of Uyea granitic gneisses and associated metagabbros in northernmost mainland of Shetland. Like all of these rocks, the Lancaster basement also lacks any geochronological or metamorphic evidence for younger Proterozoic reworking as seen in the Lewisian Complex of mainland Scotland and the Hebrides (e.g. Inverian and Laxfordian events). This confirms that the Lancaster basement belongs to the Neoarchean rocks of the Faroe–Shetland Terrane, which can be correlated with the similar age Central Greenland–Rae Craton on the NW side of the North Atlantic (Holdsworth *et al.* 2018; Kinny *et al.* 2019).

Previous researchers were unable to identify any definitive evidence for anything other than amphibolite-facies regional metamorphism in the rather sparse set of Faroe–Shetland Terrane basement samples and so it was suggested that the Neoarchean ages obtained dated primary crystallization of the igneous protoliths. Younger zircon rims formed *c.* 2700–2710 Ma in both areas were thought to possibly date the age of deformation and amphibolite-facies regional metamorphism (Kinny *et al.* 2019). It is significant that similar aged rims are also recognized in the Lancaster samples (Fig. 11). However, the charnockitic composition of the Lancaster basement rocks is consistent with granulite-facies metamorphism (e.g. Frost & Frost 2008). Given the relatively undeformed nature of the orthopyroxene-bearing tonalites, it is suggested that the *c.* 2743–2731 Ma U–Pb dates from Lancaster give the age of pluton emplacement under granulite-facies *P–T* conditions. The extent and significance of this granulite-facies event in the wider Faroe–Shetland Terrane is uncertain and requires further research. The ages obtained for this event are also very similar to those obtained for early high-grade metamorphic episodes in the Gruinard and Assynt terranes of the Lewisian Complex in mainland Scotland (Love *et al.* 2004; Crowley *et al.* 2015).

If the K–Ar age of *c.* 2308 Ma for the dolerite in 205/21a-4Z reported by Slightam (2012) is accepted, it seems likely that this intrusion represents a Scourie dyke, part of a *c.* 2400–2000 Ma regional swarm of NW–SE-trending intrusions seen cutting the gneisses of the Lewisian Complex of the Scottish mainland and Hebrides (Sutton & Watson 1951; Davies & Heaman 2014). The absence of Proterozoic Inverian and Laxfordian overprinting in the Lancaster basement, and more generally in the Faroe–Shetland Terrane, would explain the absence of a later metamorphic overprint in the sampled dolerites from this well. The intrusion is therefore of some regional significance as it represents the first potential example of a Scourie dyke identified cutting rocks of the Faroe–Shetland Terrane. More fundamentally, if its age can be proven using a more robust geochronological technique such as U–Pb zircon or baddeleyite, it will be the only UK example of a Scourie dyke that preserves a little modified primary igneous mineralogy and textures.

The age and significance of the early cataclasite–pseudotachylyte zones in the Lancaster basement is unknown, although the close association of these two fault rock types and lack of consistent overprinting relationships suggest that they are broadly contemporaneous. Similar fault rock associations are very widely recognized in the Lewisian Complex of both the Scottish mainland and the Outer Hebrides (e.g. Sibson 1977; Beacom *et al.* 2001; Imber *et al.* 2001; Park 2005). A wide range of ages has been obtained using mainly infrared laserprobe $^{40}Ar/^{39}Ar$ dating, ranging from *c.* 1900 to 430 Ma (Kelley *et al.* 1994; Sherlock *et al.* 2009). It should be noted that cataclasite and altered pseudotachylytes are also seen cutting the possible Scourie dyke dolerites in 205/21a-4Z.

Nature and ages of later mineralized fractures and fissure fills

The mineralogy and textures seen in the hydrocarbon-bearing fractures and fissure fills of the Lancaster field are very similar to those recognized all along the fractured basement of the Rona Ridge (Holdsworth *et al.* 2019). The zoned mineral fills, cockade textures and vuggy character are typical of low-temperature, near-surface hydrothermal systems, and suggest that fractures were able to remain open to the repeated upward flow of fluids for protracted periods of time (e.g. Frenzel & Woodcock 2014). The preservation of breccia, sandstone and siltstone fills to depths of many hundreds of metres also points to the existence of open fissures connected to the surface, with material introduced downwards into what are effectively cave systems by either gravity or flowing surface waters (e.g. Holland *et al.* 2011; Walker *et al.* 2011). The sidewall core samples from Lancaster therefore confirm the existence of fissures, which were first proposed based on the analysis of well image logs from the Lancaster field (e.g. Trice 2014; Belaidi *et al.* 2016).

The calcite U–Pb date of *c.* 108 Ma obtained from a relatively early calcite vein cutting basement metatonalites in 205/21a-7 suggests a latest Early Cretaceous (Aptian) age of mineralization in Lancaster. Although a little older, it is broadly consistent with Late Cretaceous calcite U–Pb ages obtained in similar mineralized fracture–fissure systems from along-strike and to the NE in the Clair field (89 ± 4 Ma) and close to the Victory field (71.9 ± 2.6 Ma) (Fig. 1a; Holdsworth *et al.* 2019). If the broad equivalence is accepted, this extends the period of fissuring, mineralization, sediment filling and active rifting to over 35 myr. This longevity seems consistent with the known persistence of the Rona Ridge as an uplifted feature that lay close to sea level throughout Jurassic to Late Cretaceous times (Ritchie *et al.* 2011; Stoker *et al.* 2018). It is perfectly possible that more than one episode of rifting, fissure formation and/or mineralization occurred during this period and it may be significant that the dated vein from 205/21a-7 is cross-cut by younger calcite-bearing fractures, which could not be dated. However, local mineralization sequences in Lancaster are seen to vary within and between wells, and also in other well cores along the Rona Ridge (see Holdsworth *et al.* 2019), and a clear and consistent sequence of events is yet to emerge. It is possible that active rifting, hydrothermal mineralization and fissure formation were episodic over a protracted time period reflecting the long-term tectonic instability in this region prior to North Atlantic break-up.

A range of temperature estimates have been obtained from fluid inclusion analyses from quartz and calcite in 205/21-1A, 205/21a-4Z and 205/21a-7. Holdsworth *et al.* (2019) reported homogenization temperatures observed in seven inclusions from calcite in 205/21-1A (4435 m) of 88–133°C (mean 115°C), whereas low homogenization temperatures (up to 90°C) were determined for calcite, quartz and K-feldspar, bearing both aqueous and oil inclusions, in 205/21a-4z (Kirk Petrophysics 2011). Temperatures

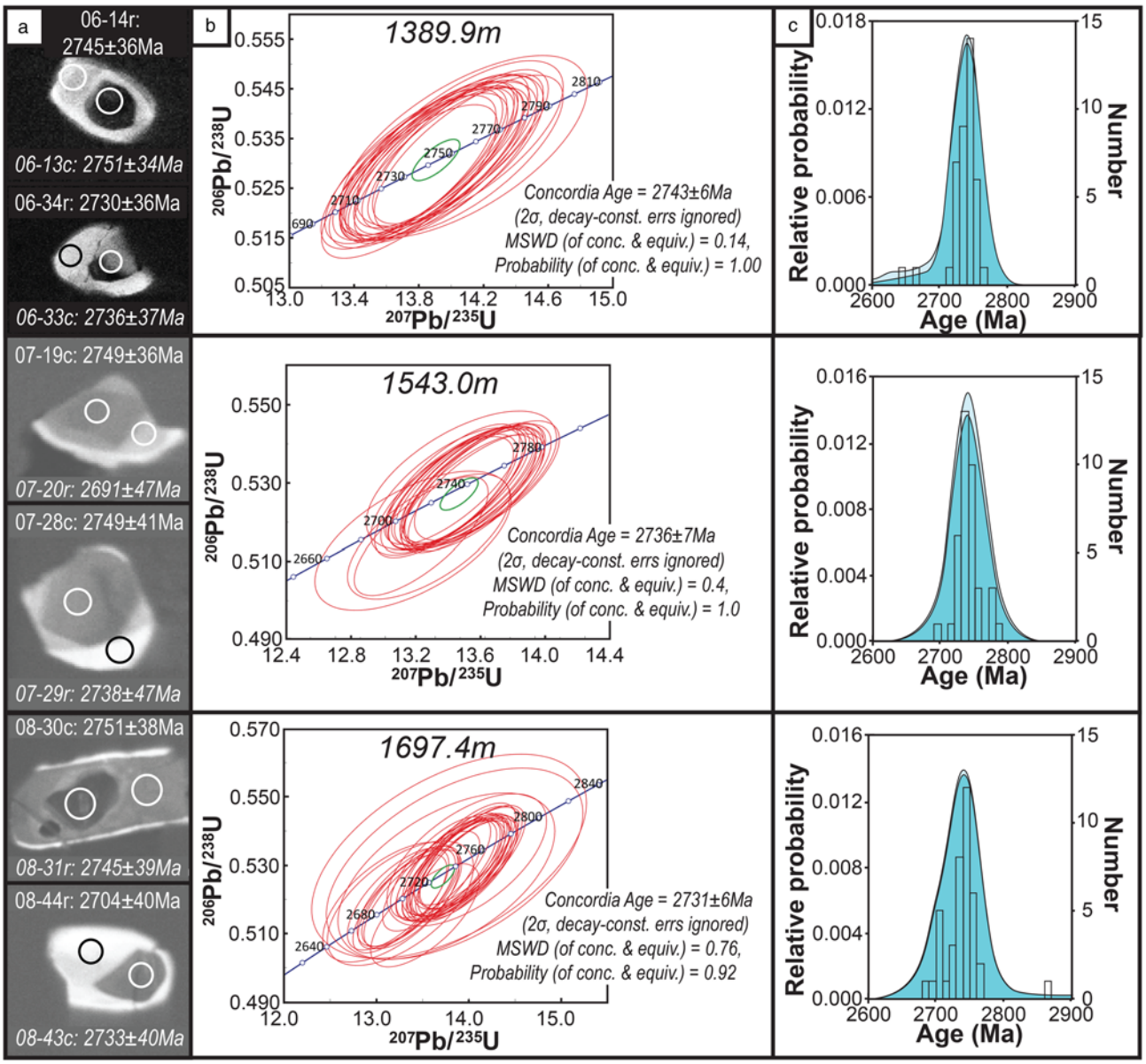

Fig. 11. U–Pb zircon geochronology from metatonalite samples at (**a**) 1389.9 m, (**b**) 1543.0 m and (**c**) 1697.4 m all from the 205/21a-7 well. (i) Representative CL images of zircons with 30 µm wide spot ages; (ii) U–Pb isotopic compositions of zircons displayed on Wetherill concordia diagrams, together with best estimates for zircon crystallization ages; all data-point error ellipses are 2σ; (iii) probability density plots of zircon ages from each of the samples.

of *c.* 142°C and 179.3°C were recorded for quartz and calcite respectively infilling a fracture from 1559.3 m in 205/21a-7 (ALS 2019*a*), whereas analyses from 1474.2 m yielded homogenization temperatures of between 185 and 192°C (mean 189°C) for nine inclusions hosted by quartz, and between 190 and 202°C (mean 197°C) for 17 inclusions hosted by calcite (ALS 2019*b*). Five inclusions in quartz and seven inclusions from calcite in 206/7a-2 in the Clair basement (2599.5 m) yielded temperatures between 214 and 218°C (mean 217°C) and 138–146°C (mean 142°C), respectively (Holdsworth *et al.* 2019). Collectively, the results are consistent with the development of fractures and mineralization at shallow depths perhaps associated with successive pulsing of hot and cold fluids with no consistent simple pattern on a regional scale.

Implications for development of the hydrocarbon reservoir

The thin-section analysis of the sidewall cores supports the validity of subdividing the fracture network into different types based on aperture to describe the hydrodynamic fracture network at Lancaster (Belaidi *et al.* 2016; Bonter *et al.* 2018). Thin-section observations in sidewall cores with lower fracture intensities suggest that the minimum effective microfracture–fracture apertures are in the region of 20 µm (Fig. 13). This minimum fracture width implies that the hydrodynamic fracture network at Lancaster will produce either oil or water and no mixed fluid transition zone will be present as irreducible water is associated with fracture widths of the order of <10 µm (Aguilera 1999).

The 'Wide Aperture Joints' identified in borehole image logs are significant as these exhibit apparent apertures in excess of 2 cm and may individually reach width of up to 2 m (Belaidi *et al.* 2016). We propose that these can be correlated with the breccia-, sediment- and mineral-filled fissures seen during the present study, many of which show significant porosities (5–10% from optical estimates in thin section, e.g. Figs 6e, 7a, d, e and 10a, b; Kirk Petrophysics 2011; ALS 2019*b*). These features have the capability to form a highly effective natural drainage network that will have extremely high permeability and potentially a high recovery factor afforded by the network connectivity (e.g. Fig. 4b). Interestingly, such aperture

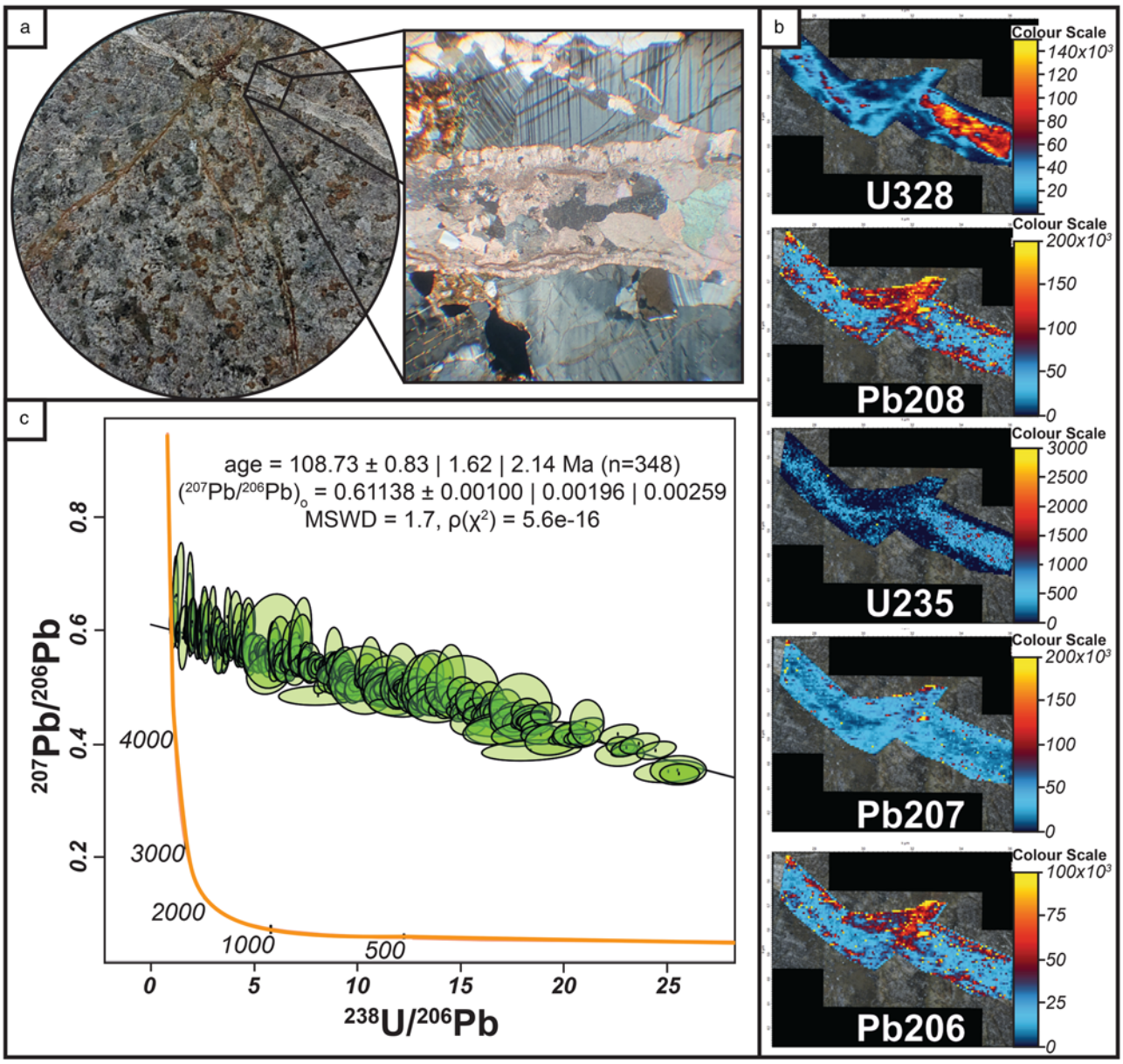

Fig. 12. (**a**) Hand sample and cross-polars thin-section view of sample A57 recovered from well 205/21a-7 at a depth of 1744 m containing a calcite vein that is crosscut by a thin hematite–calcite–clay-bearing fracture. (**b**) Isotopic maps of the calcite vein showing the concentrations of ^{238}U, ^{235}U, ^{206}Pb, ^{207}Pb and ^{208}Pb. (**c**) Tera–Wasserburg plot showing $^{238}U/^{206}Pb$ v. $^{207}Pb/^{206}Pb$ for calcite in sample A57. Age uncertainties are quoted in 2σ. MSWD, mean square of weighted deviation.

magnitudes are also characteristic of karst drainage systems seen in fractured carbonates (Esteban 1989; Trice 2005; Ford & Williams 2007) and an understanding of their genesis will be critical to evaluating the dynamic properties of the reservoir and its long-term production potential. It is important to emphasize that many faults identified from 3D seismic data (Slightam 2012) are associated with regions that have enhanced reservoir properties such as increased porosity, increased drilling gas response, increased drilling rate and increased electrical conductivity. The latter three are taken to indicate increased reservoir permeability (see Belaidi *et al.* 2016, especially their fig. 8). These Fault Zones are on average 40 m wide and form 47% of the Lancaster gross rock volume; the remaining background fractured basement is referred to as Fractured Basement (e.g. Fig. 9). 'Wide Aperture Fractures' are noted at the interfaces of Fault Zones and Fractured Basement facies (e.g. Fig. 9a) and also within Fault Zones (Fig. 9b), but they are also found less commonly in regions of Fractured Basement. Consequently, Fault Zones within the upper kilometre of the reservoir are considered to preferentially, but not exclusively, develop fissures and the associated sediment and hydrothermal mineral fills.

Figure 14 presents a simplified 3D conceptual model for the geology of the fractured basement reservoir in the Lancaster field. This uplifted block of crystalline rock may be representative of many sub-unconformity 'buried hill' traps associated with Type 1 fractured basement reservoir plays worldwide (Fig. 14a; Biddle & Wielchowsky 1994). Geological observations in actively rifting regions such as Iceland and analogue modelling studies (e.g. van Gent *et al.* 2010; von Hagke *et al.* 2019) have shown that highly dilated and interconnected fissure systems can form in mechanically strong basement rocks, such as charnockite, granite and basalt, during active extensional faulting as stresses become tensile in the uppermost crust. Thus subvertical open fissures in the upper few hundred metres closest to the surface pass down at greater depths into normal fault shear fractures dipping at *c.* 60° at depth (Fig. 14b). Following the proposals of Holdsworth *et al.* (2019; Fig. 14a), it is suggested that these open fissure systems hosted the closely

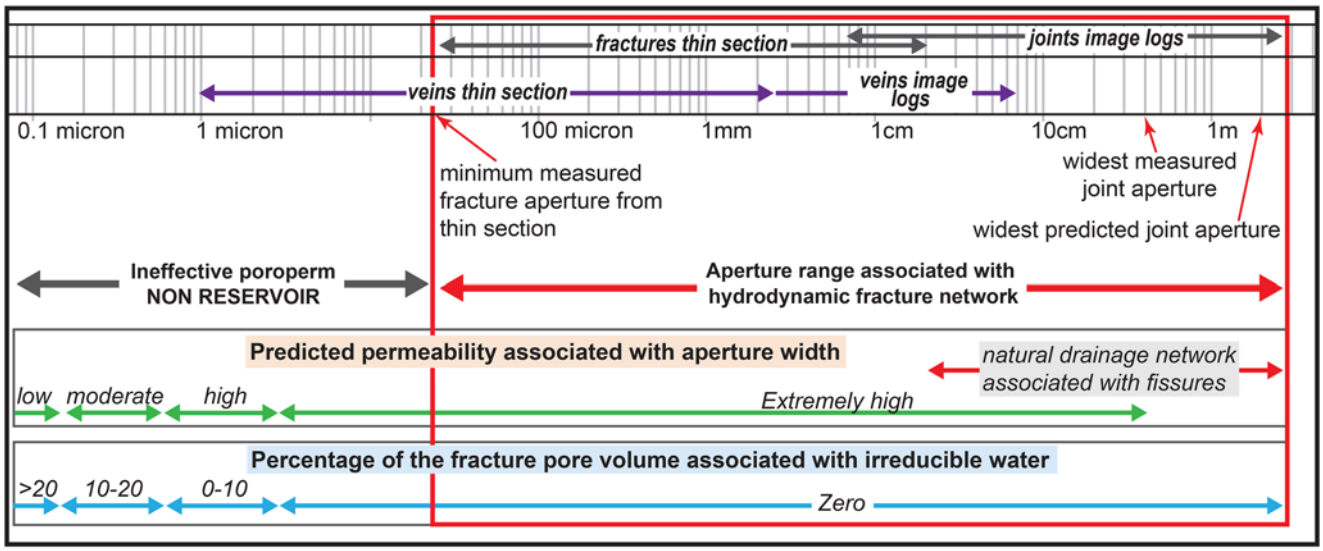

Fig. 13. Interpreted ranges of effective fracture and joint apertures estimated from thin-section and borehole image logs corrected for fracture dip and borehole attitude (modified from Belaidi *et al.* 2016). It should be noted that veins are 100% mineral-filled fractures and therefore do not contribute to reservoir porosity or permeability. The range of estimated fracture apertures is consistent with extremely high fracture permeability and zero immobile water saturation (Sw) (Aguilera 1999).

associated partial infilling of the fissures by wall rock collapse, sediment ingress (from above) and hydrothermal mineralization (from below). The widespread preservation of vuggy textures and primary porosity, and the ubiquity of zoned, cockade-style textures, is indicative of fissure systems that remained open or partially open over long time periods (Fig. 14b and c; e.g. see Lander & Laubach 2015). This very probably occurred because the partial fissure fills acted (and probably still act) as natural props holding open the fractures in the otherwise strong, low porosity–permeability basement wall rocks (Fig. 14b and c). This would allow the highly interconnected network of fissure fills to act as effective fluid storage space whilst also being able to act as long-lived fluid transport channels with preferential properties for fluid flow (Fig. 14a).

The lack of deep surficial weathering of the basement, as seen in other basement reservoirs such as the Utsira High (Riber *et al.* 2015), is consistent with the ferromagnesium mineral-poor, charnockitic composition of the metatonalites, which may have made them particularly resistant to subaerial weathering processes during the Mesozoic. Very low modern weathering rates are associated with many charnockite terrains, even in tropical environments (e.g. Gunnell & Louchet 2000). Most of the secondary alteration in these metamorphic rocks is seen to be associated with the development of the fissure systems and their associated focusing of fluid flow, both from the surface (washing in sediment) and from below (precipitation hydrothermal minerals). Thus much of the reservoir storage capacity lies in the fracture network (Fig. 14a), not in an upper zone of saprolite.

The injected slurries originating from sediment-filled fissure cavities and local preservation of oil-stained silica gels along basement-hosted shear fractures reported by Holdsworth *et al.* (2019) from the Clair Ridge have not yet been observed in the Lancaster well samples. Thus the link proposed by these researchers between fissure formation and fluid migration related to active seismicity cannot, as yet, be proven to have occurred here. However, the sudden release of elastic strain during earthquakes could lead to rapid contraction of fluid- and sediment-filled voids and account for the commonly observed development of wall-parallel foliations in many of the Lancaster fissure fills (e.g. Fig. 6d and e). Earthquake-related shaking could also trigger partial collapse of open fissure walls, leading to further partial infilling and fissure propping with breccia.

Following its relatively rapid subsidence in the Late Cretaceous, marine shales blanketed the basement ridge forming the main top and lateral seal of the buried hill trap that forms the Lancaster accumulation (Trice *et al.* 2019). It seems likely that once the naturally propped fissure systems had formed, buoyancy-driven upward migration of oil within the basement and up into local cover sequences such as the Rona Sandstone and Victory Formation below the regional shale seal was able to continue. There is very little microstructural evidence for reactivation of oil-bearing fractures in the cores, although some calcite veins and cemented clastic fissure fills in the Lancaster field may preserve evidence for late dissolution prior to infilling with oil, probably during the Cenozoic (Belaidi *et al.* 2016).

Conclusions and implications

The fractured basement reservoir of the Lancaster field is of considerable geological and economic significance. In its own right, the Neoarchean basement represents some of the best preserved charnockitic rocks in the Faroe–Shetland basement terrane and may host the only known example of a Scourie dyke with pristine igneous textures little affected by later deformation and regional metamorphic overprinting.

The large number of sidewall cores collected during exploration and appraisal of the field give detailed new insights into the geological characteristics and development of hydrocarbon-bearing fractures in what is globally a relatively unexplored play type. It illustrates that the development of tensile fissures in rheologically strong host rocks deformed near the surface during tectonic extension presents an opportunity for the development of naturally propped networks of deeply penetrating fissures that become partially to wholly filled with wall rock breccia, sediment and hydrothermal minerals. Following burial beneath a regional (or local) erosional unconformity, these fracture systems then have the potential to become sites for the accumulation and storage of significant volumes of hydrocarbons or aqueous fluids in geothermal fields/aquifers. Given that fissure formation in consolidated rocks below regional unconformities is increasingly being recognized in a variety of settings (e.g. Montenat *et al.* 1991; Frenzel & Woodcock 2014; Woodcock *et al.* 2014; Trice *et al.* 2019), it is suggested that the potential economic significance of

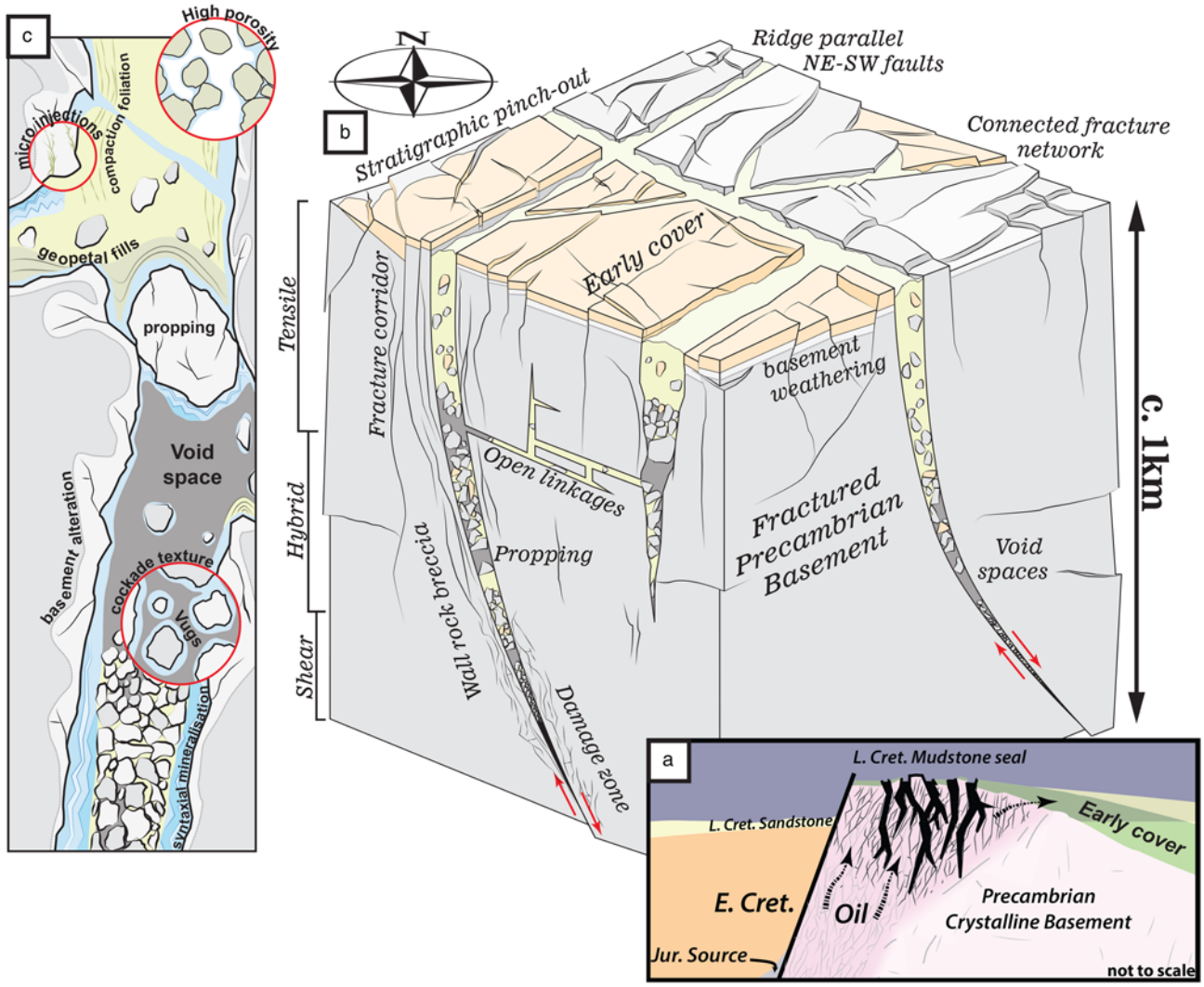

Fig. 14. (**a**) The 'buried hill' trap concept proposed by Holdsworth *et al.* (2019) for the Rona Ridge fractured basement reservoirs, including Lancaster. (**b**) Three-dimensional conceptual model of fissure fill development in the Lancaster fractured basement reservoir. (**c**) A more detailed summary of the fissure fills (wall rock clasts, sediment, mineral fills) highlighting their complex nature and role as natural proppants that hold the fissures open allowing fluid (hydrocarbon, water) ingress, migration and storage.

these features in fractured reservoirs requires further investigation as they represent natural drainage networks very similar to karst systems in fractured carbonates. Natural propping processes may also occur in a much wider range of fractured reservoirs than has previously been anticipated.

Acknowledgements C. Brown is thanked for detailed discussions concerning thin-section relationships, although the interpretations given here are solely the responsibility of the authors. Insightful and helpful reviews were provided by N. Woodcock, H. Nicholson and D. Long.

Funding Funding for this work was generously provided by Hurricane. Previous support from NERC, BP and the Clair Joint Venture partnership is also very gratefully acknowledged.

Author contributions **REH**: conceptualization (lead), funding acquisition (lead), investigation (lead), methodology (lead), project administration (lead), supervision (lead), writing - original draft (lead), writing – review & editing (equal); **RT**: conceptualization (lead), data curation (lead), funding acquisition (lead), investigation (equal), project administration (lead), resources (lead), validation (lead), writing – original draft (supporting), writing – review & editing (equal); **KH**: conceptualization (supporting), visualization (lead), writing – review & editing (supporting); **KM**: conceptualization (equal), data curation (lead), formal analysis (equal), investigation (equal), methodology (equal), writing – original draft (supporting), writing – review & editing (supporting); **AM**: conceptualization (supporting), formal analysis (supporting), investigation (supporting), writing – original draft (supporting), writing – review & editing (supporting); **DF**: data curation (supporting), formal analysis (supporting), investigation (supporting), methodology (supporting); **ED**: data curation (supporting), formal analysis (supporting), investigation (supporting), methodology (supporting), writing – review & editing (supporting); **AB**: data curation (supporting), formal analysis (supporting), investigation (supporting), methodology (supporting); **SR**: data curation (supporting), formal analysis (supporting).

Scientific editing by Danny Long

References

Aguilera, R. 1999. Recovery factors and reserves in naturally fractured reservoirs. *Journal of Canadian Petroleum Technology*, **38**, 15–18.

ALS 2019*a*. *Fluid Inclusion Studies of 5 samples from Lancaster 205/21a-7 and 5 samples from Lincoln 205/26b-12*. Confidential report prepared for Hurricane Energy, No. GB-18-J513.

ALS 2019*b*. *Thin Section Petrography of 64 Rotary Sidewall Core Samples, Lancaster Appraisal Well 205/21a-7, UKCS*. Confidential report prepared for Hurricane Energy No. ALSPRO17/029-3.

Beacom, L.E., Holdsworth, R.E., McCaffrey, K.J.W. & Anderson, T.B. 2001. A quantitative study of the influence of pre-existing compositional and fabric heterogeneities upon fracture-zone development during basement reactivation. *In*: Holdsworth, R.E., Strachan, R.A., Magloughlin, J.F. & Knipe, R.J. (eds) *The Nature and Tectonic Significance of Fault Zone Weakening*. Geological Society, London, Special Publications, **186**, 195–211, https://doi.org/10.1144/GSL.SP.2001.186.01.12

Belaidi, A., Bonter, D.A., Slightam, C. & Trice, R.C. 2016. The Lancaster Field: progress in opening the UK's fractured basement play. *In*: Bowman, M. & Levell, B. (eds) *Petroleum Geology of NW Europe: 50 Years of Learning – Proceedings of the 8th Petroleum Geology Conference*. Geological Society, London, 385–398, https://doi.org/10.1144/PGC8.20

Biddle, K.T. & Wielchowsky, C.C. 1994. Hydrocarbon Traps: Chapter 13: Part III. Processes. *In*: Magoon, L. & Dow, W. (eds) *The Petroleum System – From Source To Trap*. AAPG, Memoirs, **60**, 219–235.

Bonnet, E., Bour, O., Odling, N.E., Davy, P., Main, I., Cowie, P. & Berkowitz, B. 2001. Scaling of fracture systems in geological media. *Reviews of Geophysics*, **39**, 347–383, https://doi.org/10.1029/1999RG000074

Bonter, D., Trice, R., Cavalleri, C., Delius, H. & Singh, K. 2018. Giant oil discovery West of Shetland – challenges for fractured basement formation evaluation. SPWLA 59th Annual Logging Symposium, 2–6 June, London, Society of Petrophysicists and Well-Log Analysts, https://www.onepetro.org/conference-paper/SPWLA-2018-M

Chambers, L., Darbyshire, F., Noble, S. & Ritchie, D. 2005. *NW UK continental margin: chronology and isotope geochemistry*. British Geological Survey, Commissioned Report, **CR/05/095**.

Coney, D., Fyfe, T.B., Retail, P. & Smith, P.J. 1993. Clair Appraisal – the benefits of a co-operative approach. *In*: Parker, J.R. (ed.) *Petroleum Geology of Northwest Europe: Proceedings of the 4th Conference*. Geological Society, London, 1409–1420, https://doi.org/10.1144/0041409

Crowley, Q.C., Key, R. & Noble, S.R. 2015. High-precision U–Pb dating of complex zircon from the Lewisian Gneiss Complex of Scotland using an incremental CA-ID-TIMS approach. *Gondwana Research*, **27**, 1381–1391, https://doi.org/10.1016/j.gr.2014.04.001

Cuong, T.X. & Warren, J.K. 2009. Bach Ho Field, a fractured granitic basement reservoir, Cuu Long Basin, offshore SE Vietnam – a 'buried-hill' play. *Journal of Petroleum Geology*, **32**, 129–156, https://doi.org/10.1111/j.1747-5457.2009.00440.x

Davies, J.H.F.L. & Heaman, L.M. 2014. New U–Pb baddeleyite and zircon ages for the Scourie dyke swarm: a long-lived large igneous province with implications for the Palaeoproterozoic evolution of NW Scotland. *Precambrian Research*, **249**, 180–198, https://doi.org/10.1016/j.precamres.2014.05.007

Dempsey, E.D., Holdsworth, R.E., Imber, J., Bistacchi, A. & Di Toro, G. 2014. A geological explanation for intraplate earthquake clustering complexity: The zeolite-bearing fault/fracture networks in the Adamello Massif (Southern Italian Alps). *Journal of Structural Geology*, **66**, 58–74, https://doi.org/10.1016/j.jsg.2014.04.009

Esteban, M. 1989. *Paleokarst reservoirs in unconformity plays; strategies and applications to Miocene reefs*. Erico Petroleum Information, Jakarta.

Finlay, A., Selby, D. & Osborne, M. 2011. Re–Os geochronology and fingerprinting of United Kingdom Atlantic margin oil: temporal implications for regional petroleum systems. *Geology*, **39**, 475–478, https://doi.org/10.1130/G31781.1

Ford, D. & Williams, P. 2007. *Karst Hydrogeology and Geomorphology*. Wiley, Chichester.

Frenzel, M. & Woodcock, N.H. 2014. Cockade breccia: product of mineralisation along dilational faults. *Journal of Structural Geology*, **68**, 194–206, https://doi.org/10.1016/j.jsg.2014.09.001

Frost, B.R. & Frost, C.D. 2008. On charnockites. *Gondwana Research*, **13**, 30–44, https://doi.org/10.1016/j.gr.2007.07.006

Gunnell, Y. & Louchet, A. 2000. The influence of rock hardness and divergent weathering on the interpretation of apatite fission-track denudation rates. Evidence from charnockites in South India and Sri Lanka. *Zeitschrift für Geomorphologie*, **44**, 33–57.

Gutmanis, J.C. 2009. Basement reservoirs – a review of their geological and production histories. International Petroleum Technology Conference held in Doha, Qatar, 7–9 December, IPTC 13156, https://doi.org/10.2523/IPTC-13156-MS

Holdsworth, R.E., Morton, A. *et al.* 2018. The nature and significance of the Faroe–Shetland Terrane: linking Archaean basement blocks across the North Atlantic. *Precambrian Research*, **321**, 154–171, https://doi.org/10.1016/j.precamres.2018.12.004

Holdsworth, R.E., McCaffrey, K.J.W. *et al.* 2019. Natural fracture propping and earthquake-induced oil migration in fractured basement reservoirs. *Geology*, **47**, 700–704, https://doi.org/10.1130/G46280.1

Holland, M., Van Gent, H.W., Bazalgette, L., Yassir, N., Hoogerduijn-Strating, E.H. & Urai, J.L. 2011. Evolution of dilatant fracture networks in normal faults – evidence from 4D model experiments. *Earth and Planetary Science Letters*, **304**, 399–406, https://doi.org/10.1016/j.epsl.2011.02.017

Holmes, A.J., Griffith, C.E. & Scotchman, I.C. 1999. The Jurassic petroleum system of the West of Britain Atlantic margin – an integration of tectonics, geochemistry, and basin modelling. *In*: Fleet, A.J. & Boldy, S.A.R. (eds) *Petroleum Geology of Northwest Europe: Proceedings of the 5th Conference*. Geological Society, London, 1351–1365, https://doi.org/10.1144/0051351

Imber, J., Holdsworth, R.E., Butler, C.A. & Strachan, R.A. 2001. A reappraisal of the Sibson–Scholz fault zone model: the nature of the frictional to viscous ('brittle–ductile') transition along a long-lived, crustal-scale fault, Outer Hebrides, Scotland. *Tectonics*, **20**, 601–624, https://doi.org/10.1029/2000TC001250

Kelley, S.P., Reddy, S.M. & Maddock, R. 1994. Laser-probe $^{40}Ar/^{39}Ar$ investigation of a pseudotachylyte and its host rock from the Outer Isles thrust, Scotland. *Geology*, **22**, 443–446, https://doi.org/10.1130/0091-7613(1994)022<0443:LPAAIO>2.3.CO;2

Kinny, P.D., Strachan, R.A. *et al.* 2019. The Neoarchean Uyea Gneiss Complex, Shetland: an onshore fragment of the Rae Craton on the European Plate. *Journal of the Geological Society, London*, https://doi.org/10.1144/jgs2019-017

Kirk Petrophysics 2011. *Petrographic and Fluid Inclusion Study of the Lewisian Basement of Lancaster Prospect Well 205/21a-4z*. Confidential report prepared for Hurricane Exploration, No. KP10004-3.

Koenders, M.A. & Petford, N. 2003. Thermally induced primary fracture development in tabular granitic plutons: a preliminary analysis. *In*: Petford, N. & McCaffrey, K.J.W. (eds) *Hydrocarbons in Crystalline Rocks*. Geological Society, London, Special Publications, **214**, 143–150, https://doi.org/10.1144/GSL.SP.2003.214.01.09

Koning, T. 2003. Oil production from basement reservoirs: examples from Indonesia, USA and Venezuela. *In*: Petford, N. & McCaffrey, K.J.W. (eds) *Hydrocarbons in Crystalline Rocks*. Geological Society, London, Special Publications, **214**, 83–92, https://doi.org/10.1144/GSL.SP.2003.214.01.05**

Lander, R.H. & Laubach, S.E. 2015. Insights into rates of fracture growth and sealing from a model for quartz cementation in fractured sandstones. *Geological Society of American Bulletin*, **127**, 516–538, https://doi.org/10.1130/B31092.1

Love, G.J.L., Kinny, P.D. & Friend, C.R.L. 2004. Timing of magmatism and metamorphism in the Gruinard Bay area of the Lewisian Gneiss Complex: comparisions with the Assynt Terrane and implications for terrane accretion. *Contributions to Mineralogy and Petrology*, **146**, 620–636, https://doi.org/10.1007/s00410-003-0519-1

Montenat, C., Barrier, P. & Ottd'Estevou, P. 1991. Some aspects of the recent tectonics in the Strait of Messina, Italy. *Tectonophysics*, **194**, 203–215, https://doi.org/10.1016/0040-1951(91)90261-P

P'an, C.H. 1982. Petroleum in basement rocks. *AAPG Bulletin*, **66**, 1597–1643.

Park, R.G. 2005. The Lewisian terrane model: a review. *Scottish Journal of Geology*, **41**, 105–118, https://doi.org/10.1144/sjg41020105

Passchier, C.W. & Trouw, R.A.J. 2005. *Microtectonics*, 2nd edn. Springer, Berlin.

Psyrillos, A., Burley, S.D., Manning, D.A.C. & Fallick, A.E. 2003. Coupled mineral–fluid evolution of a basin and high: kaolinization in the SW England granites in relation to the development of the Plymouth Basin. *In*: Petford, N. & McCaffrey, K.J.W. (eds) *Hydrocarbons in Crystalline Rocks*. Geological Society, London, Special Publications, **214**, 175–195, https://doi.org/10.1144/GSL.SP.2003.214.01.11

Riber, L., Dypvik, H. & Sørlie, R. 2015. Altered basement rocks on the Utsira High and its surroundings, Norwegian North Sea. *Norwegian Journal of Geology*, **93**, 57–89.

Riber, L., Dypvik, H., Sørlie, R., Naqvis, A.M., Stangvik, K., Oberhardt, N. & Schroeder, P.A. 2017. Comparison of deeply buried palaeoregolith profiles, Norwegian North Sea, with outcrops from southern Sweden and Georgia, USA – implications for petroleum exploration. *Palaeogeography, Palaeoclimatology, Palaeoecology*, **471**, 82–95, https://doi.org/10.1016/j.palaeo.2017.01.043

Ritchie, J.D., Ziska, H., Johnson, H. & Evans, D. 2011. *Geology of the Faroe–Shetland Basin and adjacent areas*. British Geological Survey Research Report, **RR/11/01**.

RPS 2017. *Evaluation of Lancaster Field within Licence P.1368 on behalf of Hurricane Energy plc*. Competent Persons Report, **ECV2210**.

Sanderson, D. & Nixon, C. 2015. The use of topology in fracture network characterization. *Journal of Structural Geology*, **72**, 55–66, https://doi.org/10.1016/j.jsg.2015.01.005

Seeburger, D.A. & Zoback, M.D. 1982. The distribution of natural fractures and joints at depth in crystalline rock. *Journal of Geophysical Research*, **87**, 5517–5534, https://doi.org/10.1029/JB087iB07p05517

Sherlock, S.C., Strachan, R.A. & Jones, K.A. 2009. High spatial resolution $^{40}Ar/^{39}Ar$ dating of pseudotachylites: geochronological evidence for multiple phases of faulting within basement gneisses of the Outer Hebrides. *Journal of the Geological Society, London*, **166**, 1049–1059, https://doi.org/10.1144/0016-76492008-125

Sibson, R.H. 1977. Fault rocks and fault mechanisms. *Journal of the Geological Society, London*, **133**, 191–213, https://doi.org/10.1144/gsjgs.133.3.0191

Slightam, C. 2012. Characterizing seismic-scale faults pre- and post-drilling; Lewisian Basement, West of Shetlands, UK. *In*: Spence, G.H., Redfern, J., Aguilera, R., Bevan, T.G., Cosgrove, J.W., Couples, G.D. & Daniel, J.M. (eds) *Advances in the Study of Fractured Reservoirs*. Geological Society, London, Special Publications, **374**, 311–332, https://doi.org/10.1144/SP374.6

Stoker, M.S., Holford, S.P. & Hillis, R.R. 2018. A rift-to-drift record of vertical crustal motions in the Faroe–Shetland Basin, NW European margin: establishing constraints on NE Atlantic evolution. *Journal of the Geological Society, London*, **175**, 263–274, https://doi.org/10.1144/jgs2017-076

Sutton, J. & Watson, J. 1951. The pre-Torridonian metamorphic history of the Loch Torridon and Scourie areas in the north-west Highlands, and its bearing on the chronological classification of the Lewisian. *Quarterly Journal of the Geological Society*, **106**, 241–307, https://doi.org/10.1144/GSL.JGS.1950.106.01-04.16

Trice, R. 2005. Challenges and insights of optimising oil production from Middle East mega karst reservoirs. Society of Petroleum Engineers, SPE-93679-MS, https://doi.org/10.2118/93679-MS

Trice, R. 2014. Basement exploration West of Shetlands, progress in opening a new play on the UKCS. *In*: Cannon, S.J.C. & Ellis, D. (eds)

Hydrocarbon Exploration to Exploitation West of Shetlands. Geological Society, London, Special Publications, **397**, 81–105, https://doi.org/10.1144/SP397.3

Trice, R., Holdsworth, R.E., Rogers, S. & McCaffrey, K.J. 2018. Characterising the fracture properties of Lewisian Gneiss basement reservoirs, Rona Ridge, West of Shetland. *In*: *The Geology of Fractured Reservoirs, 24–25 October, London. Programme and Abstract Volume*. Geological Society Petroleum Group, London, 55.

Trice, R., Hiorth, C. & Holdsworth, R.E. 2019. Fractured basement play development in the UK and Norwegian rifted margins: a discussion and implications for exploitation. *In*: Jackson, C.A.-L. (ed.) *Cross-Border Petroleum Geology and Exploration: The British and Norwegian Continental Margins*. Geological Society, London, Special Publications, https://doi.org/10.1144/SP495-2018-174

van Gent, H.W., Holland, M., Urai, J.L. & Loosveld, R. 2010. Evolution of fault zones in carbonates with mechanical stratigraphy – insights from scale models using layered cohesive powder. *Journal of Structural Geology*, **32**, 1375–1391, https://doi.org/10.1016/j.jsg.2009.05.006

von Hagke, C., Kettermann, M., Bitsch, N., Bücken, D., Weismüller, C. & Urai, J.L. 2019. The effect of obliquity of slip in normal faults on distribution of open fractures. *Frontiers in Earth Science*, **7**, 18, https://doi.org/10.3389/feart.2019.00018

Walker, R.J., Holdsworth, R.E., Imber, J. & Ellis, D. 2011. The development of cavities and clastic infills along fault-related fractures in Tertiary basalts on the NE Atlantic margin. *Journal of Structural Geology*, **33**, 92–106, https://doi.org/10.1016/j.jsg.2010.12.001

Witt, A.J., Fowler, S.R., Kjelstadli, R.M., Draper, L.F., Barr, D. & McGarrity, J.P. 2011. Managing the start-up of a fractured oil reservoir: development of the Clair field, West of Shetland. *In*: Vining, B.A. (ed.) *Petroleum Geology: From Mature Basins to New Frontiers – Proceedings of the 7th Petroleum Geology Conference*. Geological Society, London, 299–313, https://doi.org/10.1144/0070299

Woodcock, N.H., Miller, A.V. & Woodhouse, C.D. 2014. Chaotic breccia zones on the Pembroke Peninsula, South Wales: collapse into voids along dilational faults. *Journal of Structural Geology*, **69**, 91–107, https://doi.org/10.1016/j.jsg.2014.09.019